GBT Memo No. 322

GBT L-band Investigation with Physical Optics Modeling and SEFD Analysis

Steven White, Robert Simon, Walter Klahold, Laura Leyzorek

Introduction

Painting of the GBT upper feed arm required removal of all feeds and receivers. This opportunity allowed time for testing, calibration, and a comparison with CST modeling results. A GBT Gregorian model is developed in the TICRA/GRASP physical optics package to calculate GBT gain (total efficiency) and total spill over. Since L band is typically inaccessible, most of the effort was devoted to characterizing this receiver. Particular attention is directed toward investigation of low-level baseline instabilities primarily in the XL channel. A comprehensive S-parameter characterization and EM modeling of components, and characterization of the LNA noise properties and S parameters at cryogenic temperatures are presented. Although previous measurements of the feed and OMT were available, presumably in the OTF building, the test parameters and methodology were not well documented, thus there was no attempt to recreate these measurements given the difficulty in mounting the feed. A system noise temperature divided by efficiency is predicted based on the results and compared to GBT SEFD measurements. Details of the GRASP model construction for the Gregorian focus are also given.

Baseline Ripple

Observing reports have alluded to a low-level baseline ripple present in the GBT L-band receiver primarily in the XL channel. Karen O'Neil's RFI scans show the difference in YR and XL in Figure 1. Inspection of the components, particularly the stainless-steel cables, gave no indication of damage, thus left intact. Replacing these would require a characterization of the phase delays, a time consuming and difficult task. The only obvious difference in the two channels is the return loss of the cryogenic low noise amplifier in YR, serial number L129, greater by ~10 dB than XL, L108, as shown in Figure 2. For this reason, amplifier, L22 was installed. This amplifier has similar return loss to L129 and a lower measured noise temperature. [1]

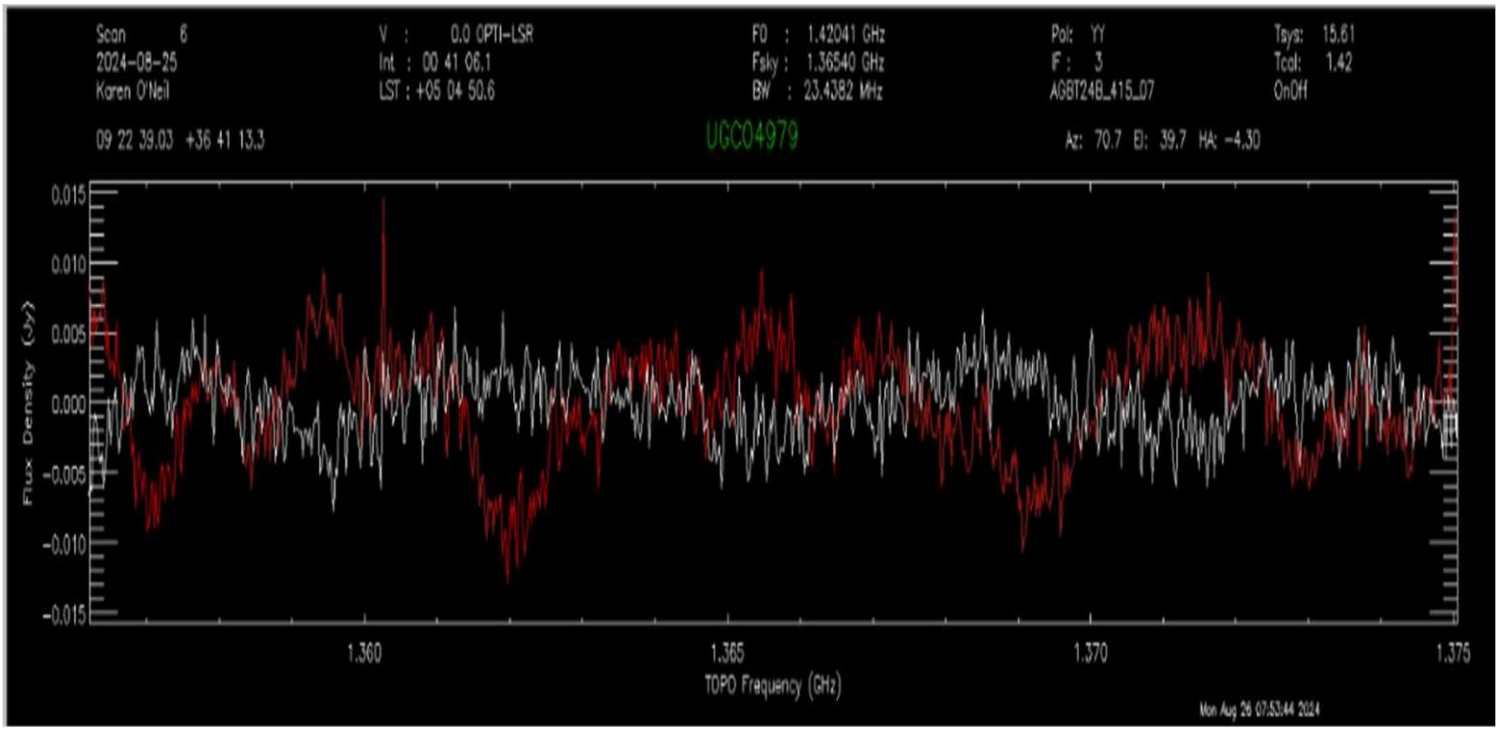

Figure 1 RFI investigation shows greater baseline ripple in XL (red), than YL (white).

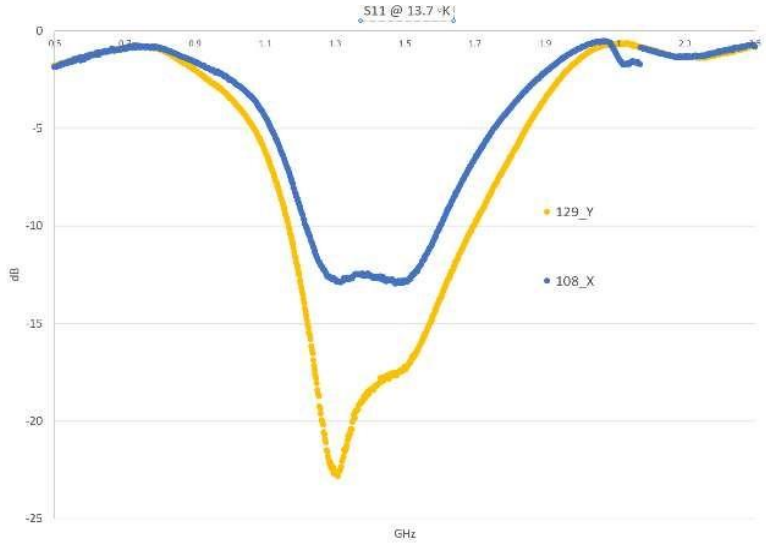

Figure 2. S11 comparison for L-band cryogenic amplifiers L129 (yellow), and L108 (blue).

VNA: S-parameter Tests

Initial testing of the OMT showed lower return loss than the Stennes measurements. [2] This warranted further investigation as the exact methodology of these measurements are unknown. Available L-band test components are listed in the Table: Photographs:4-14. Various combinations of test adapters were configured for the OMT to reproduce the Srikanth 1996 Indoor/Outdoor Test Building measurements. [3,4] CST models of the OMT with coaxial to waveguide transitions, as show in Figure 3, confirmed impedance match limitation of the stepped impedance transformer from circular to WR650 rectangular wave guide. The modeled S-parameter results of the OMT are shown in Figure 4, where port one is the circular waveguide, and port three is

the polarization aligned coaxial port. The Stennes and Shrikanth plots show lower return loss and higher isolation than the current modeled or measured results.

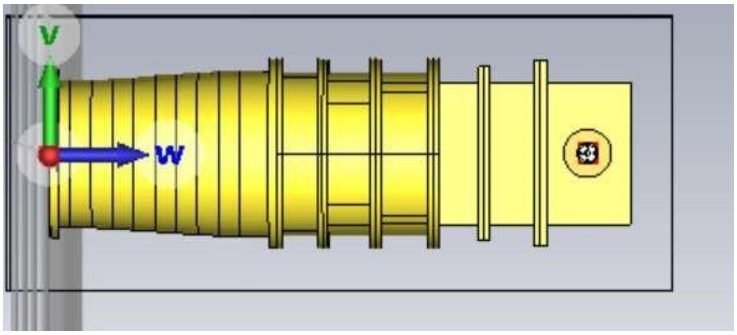

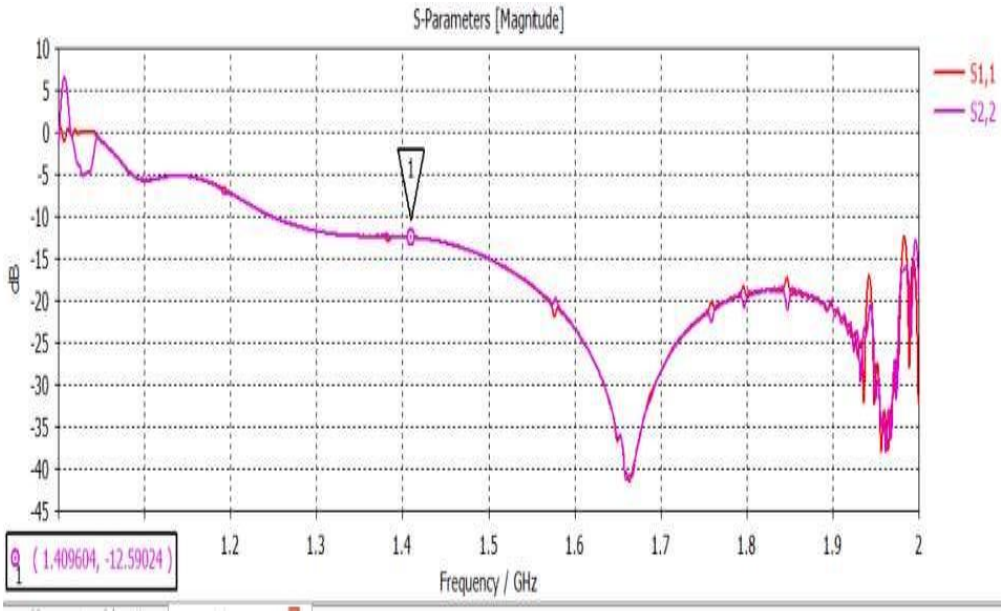

Figure 3. CST model S-parameter results of L band coaxial to circular waveguide transitions, Port 1 is waveguide, Port 2 is coaxial (N type).

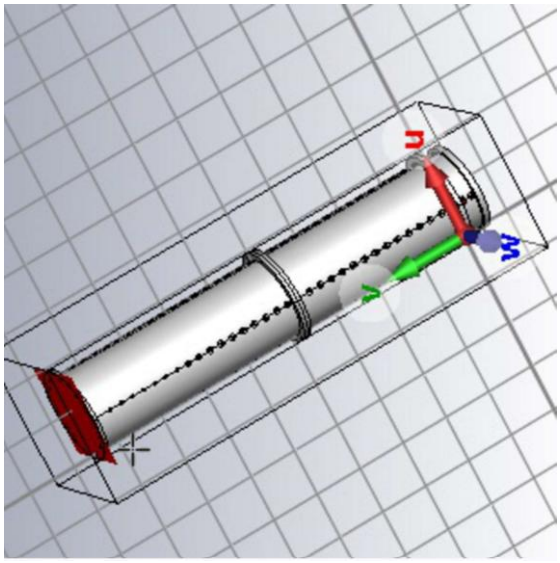

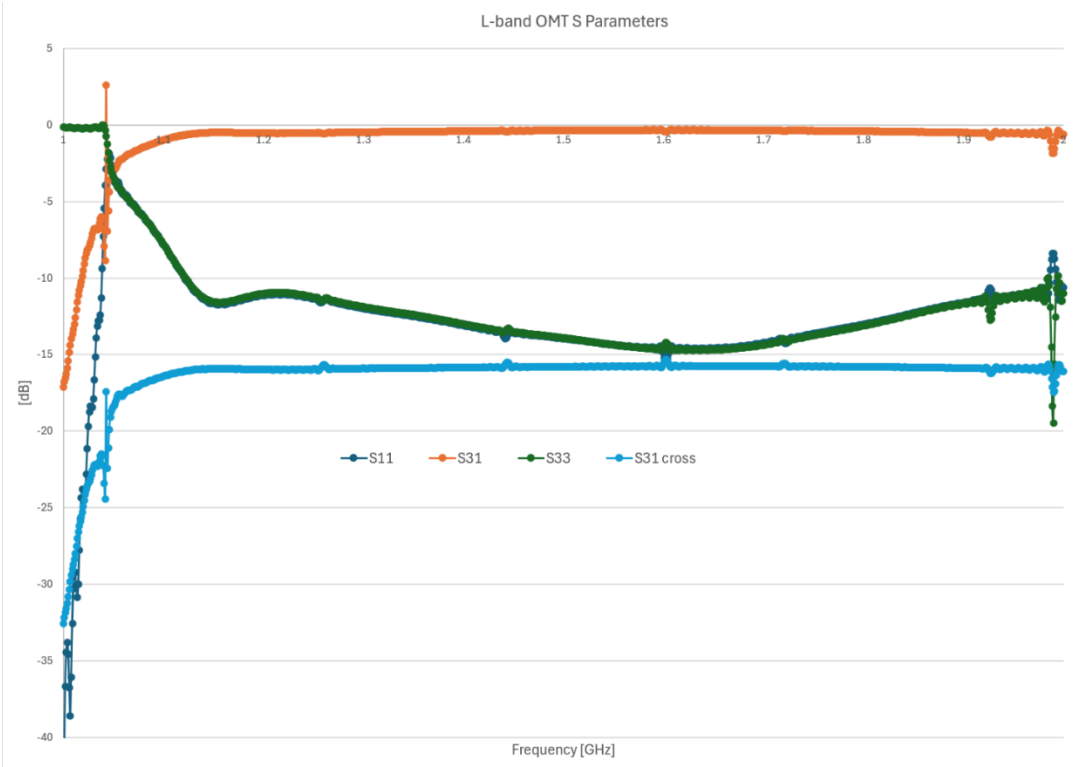

Figure 4. CST model (top) showing first order mode S-parameter results (S1(1),1(1) blue; S3(1),3(1) green; S3(1),1(1) orange; S3(1),1(2) cross cyan) of L band OMT: Port 1 is waveguide, Port 2 is coaxial (SMA) cross polarized, Port 3 is coaxial (SMA) co-polarization.

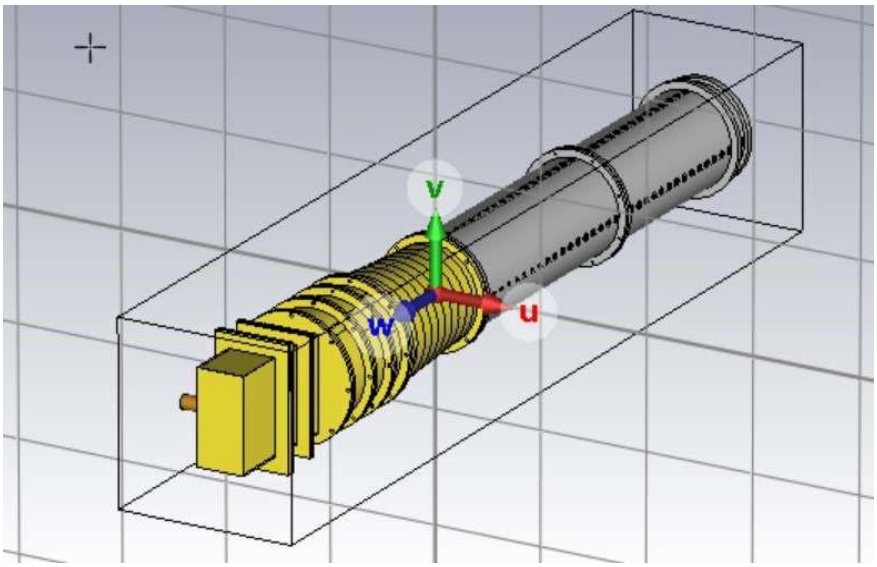
v
w
u

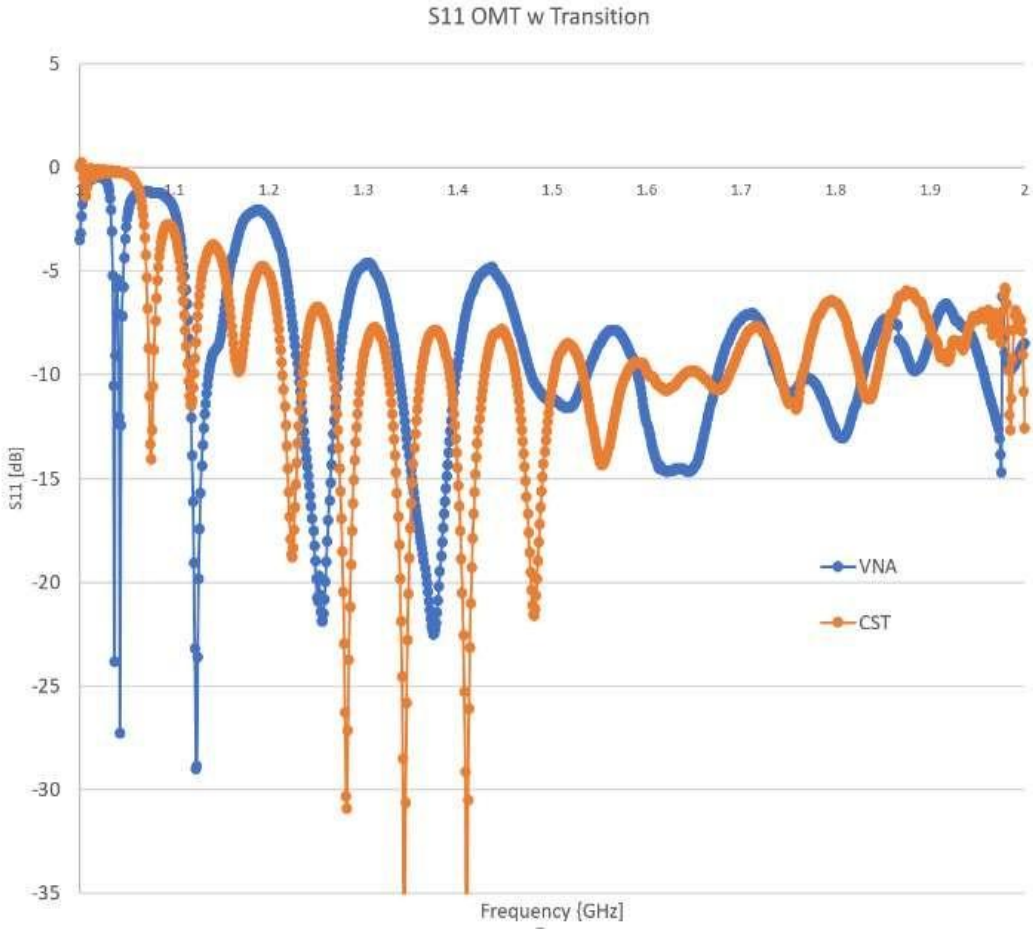
S11 OMT w Transition
5
0
-5
-10
-15
-20
-25
-30
-35
S11 [dB]
1.1
1.2
1.3
1.4
1.5
1.6
1.7
1.8
1.9
2
VNA
CST
Frequency [GHz]

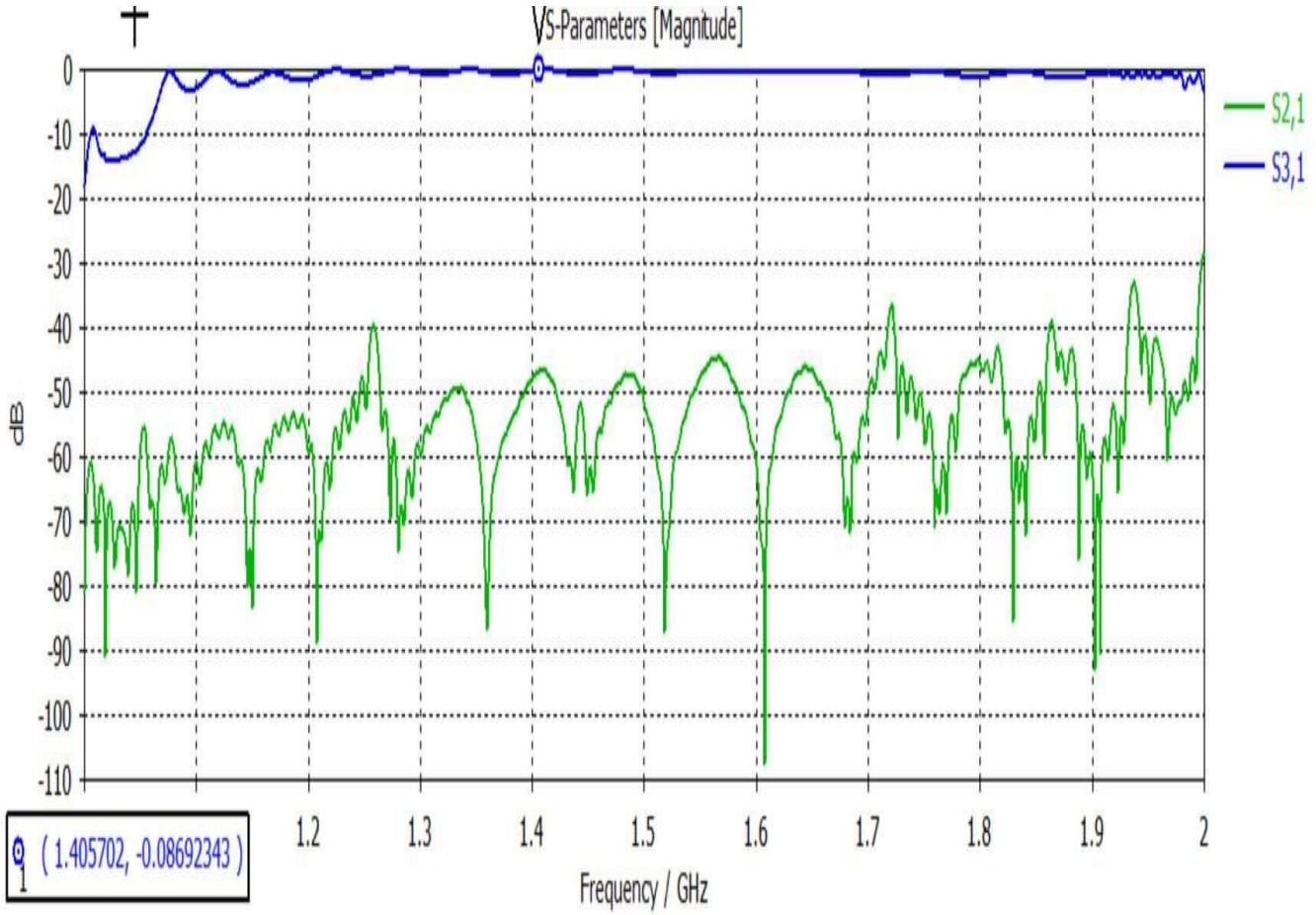

Figure 5. CST model (top), corresponding return loss for the circular waveguide port (middle), and insertion losses from the circular ports to the coaxial ports (bottom). The return loss is shown for both the simulated results from CST (orange) and measured data on the lab VNA (blue). The insertion loss shows simulated data from CST only. The port indices in all plots are, 1=circular waveguide port, 2=coaxial port anti-aligned with coaxial-to-waveguide adapter, 3=coaxial port aligned with coaxial-to-waveguide adapter.

CST Model vs VNA Measurements: Feed Assembly

The GBT feed was assembled for laboratory testing of Figure 6 with a pyramidal absorber over the feed for impedance matching. A combination of hoist, straps, roll carts, and lab jacks provided the alignment necessary for assembly. With a VNA two port coaxial calibration, the measured return loss was less than the model predicted as shown in the plots of Figure 7. The conclusion is that size limitation of space made placement of the absorber awkward so that achieving a good match was not possible. The placement of the absorber near the aperture is also suspect and has consequences on GBT tests with the absorber placed directly on the feed. Time limitations likely will not allow installation of the feed warm to facilitate GBT VNA tests but is recommended if the opportunity permits.

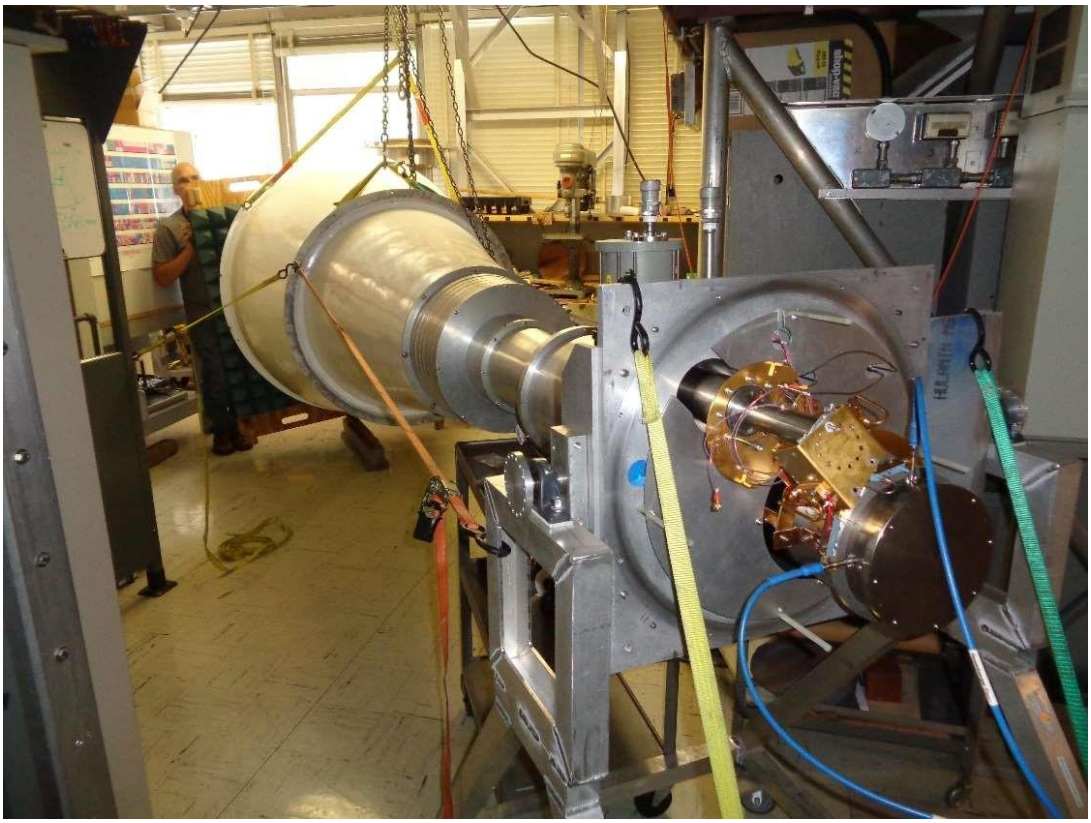

C-RAM™ SFC

High performance broadband pyramidal RF absorber

GRADE	HEIGHT in. (mm)	WEIGHT lbs. (kg)	TIPS Per Piece	TYPICAL REFLECTIVITY AT FREQUENCY IN GHz (Minimum reflectivity at frequency in GHz)										
				0.08	0.10	0.3	0.5	1.0	3.0	6.0	10	18	36*	50*
SFC-8	8 (203)	4.5 (2.0)	64					-30 (-30)	-40 (-34)	-50 (-45)	-59 (-50)	-60 (-50)	-50	-50
SFC-12	12 (305)	6 (2.7)	36					-38 (-33)	-55 (-37)	-60 (-45)	-60 (-50)	-60 (-50)	-50	-50

Figure 6. S11 measurements in the lab, showing the receiver at room temperature, with feed horn attached, and 300K SFC-8 absorber over feed aperture. The absorber is expected to have better than -30 dB reflectivity; however, the measurements indicate that the proximity of the absorber to the aperture results in much higher reflectivity. Directly above are specifications for a similar absorber. The exact specifications are unknown for this sample.

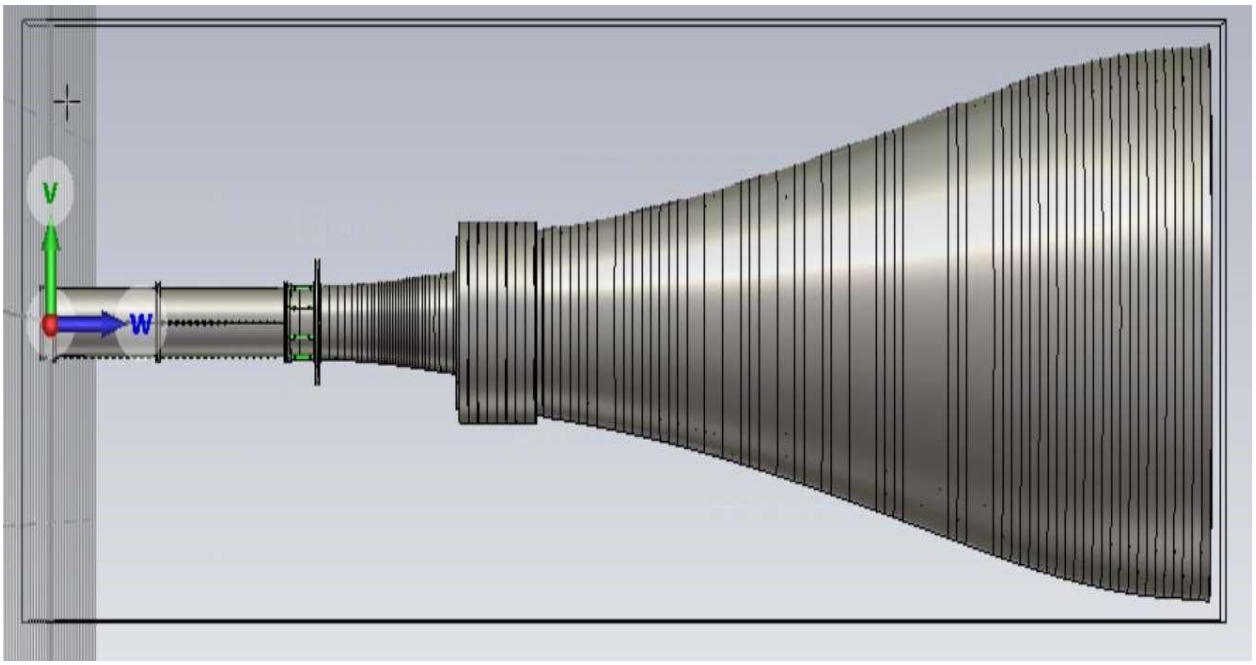
V
W

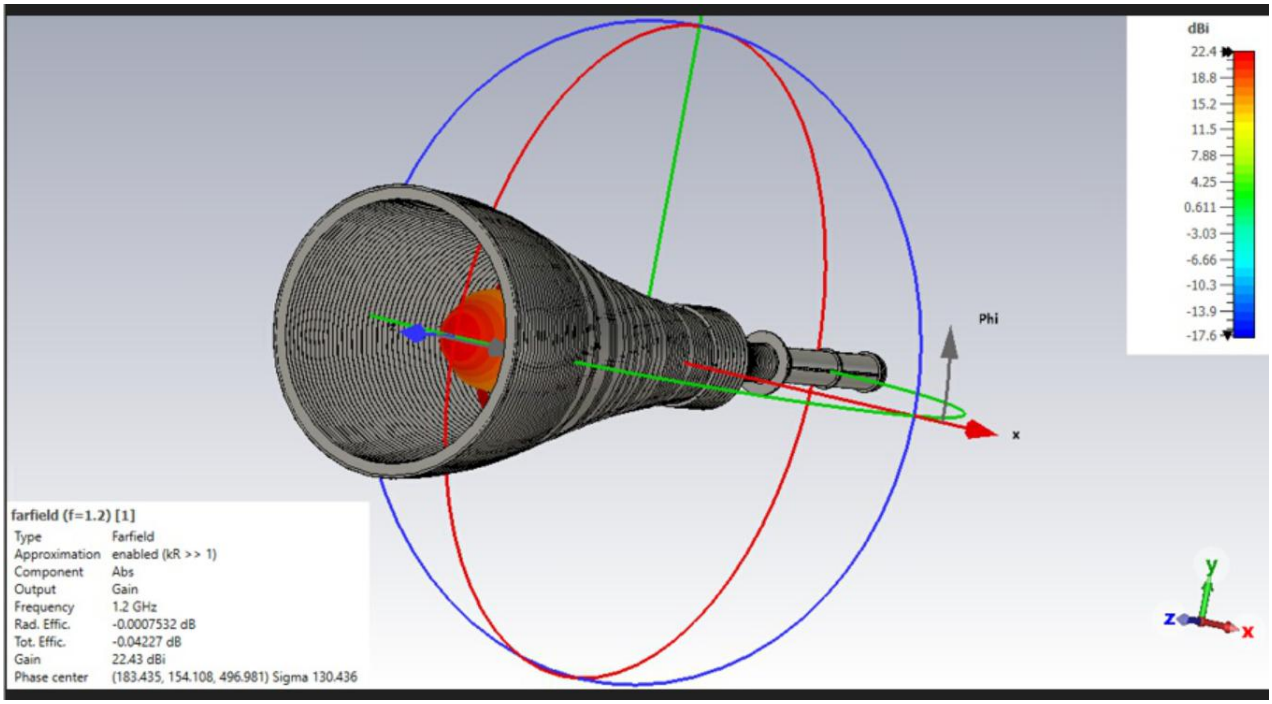
dBi
22.4
18.8
15.2
11.5
7.88
4.25
0.611
-3.03
-6.66
-10.3
-13.9
-17.6
Phi
x
farfield (f=1.2) [1]
Type Farfield
Approximation enabled (kR >> 1)
Component Abs
Output Gain
Frequency 1.2 GHz
Rad. Effic. -0.0007532 dB
Tot. Effic. -0.04227 dB
Gain 22.43 dBi
Phase center (183.435, 154.108, 496.981) Sigma 130.436
y
z
x

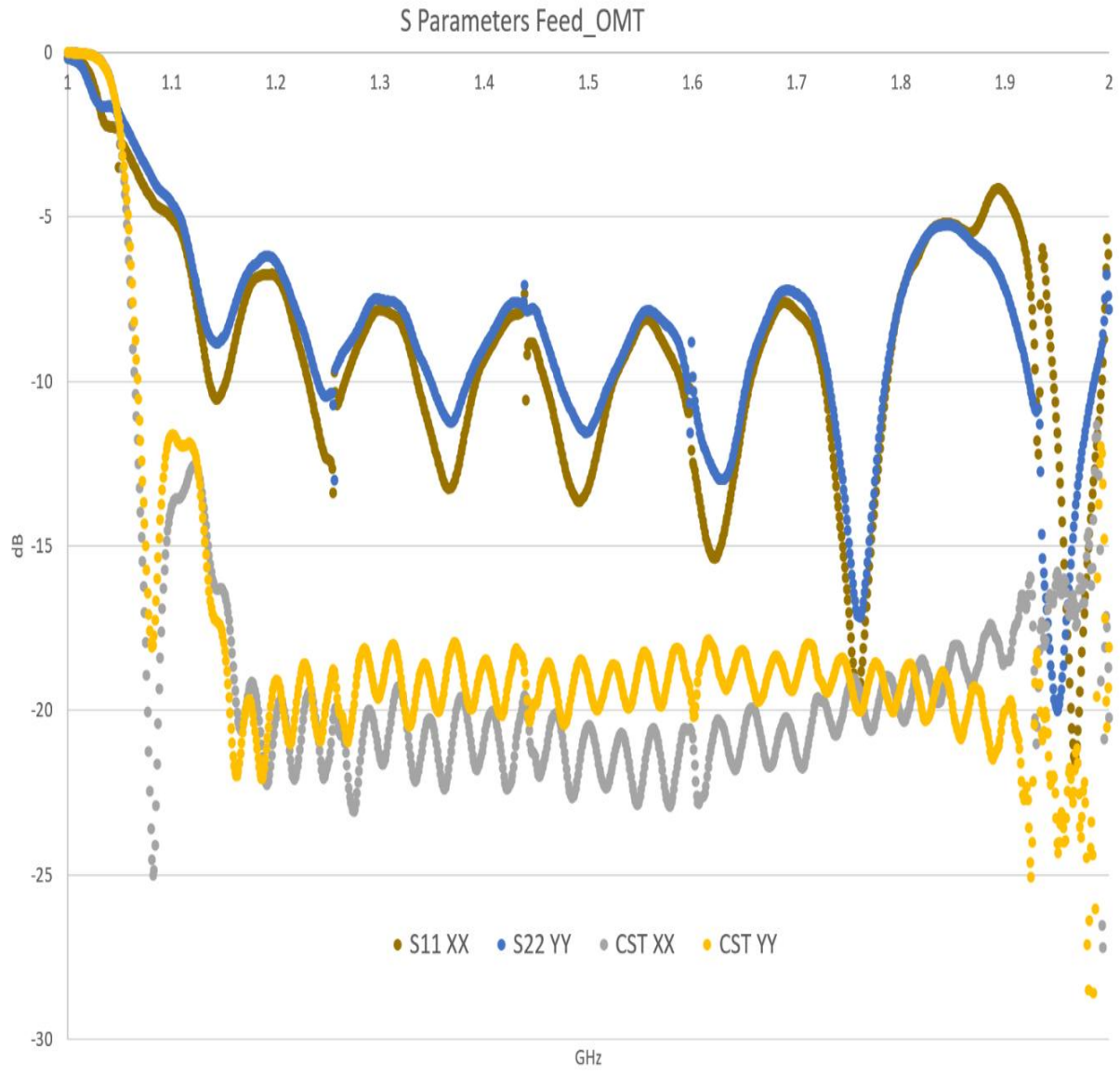

Figure 7. VNA measurements versus CST model comparison of the L band feed with OMT with transition. S11 for polarization YR (blue), and S22 for polarization XL (brown). The probe for XL is above the YR probe and located closer to the aperture. These measurements compare with reference 2. Of note is the CST phase center location calculated at 1.2 GHz. This corresponds to the mounting ring location of reference 3. All CST far fields are exported with this coordinate origin.

TICRA/GRASP with CST Model Far Field Results

The CST model, Files: EM Modeling.2, is constructed with the as built drawings for the OMT and feed horn listed in Table Files: Excel.3, imported from Inventor models. The far field computations are exported to the TICRA/GRASP model for the GBT. Three GRASP models were compared. One is adapted from the GBT Radar project "Array Main Dish" rendition. This model analysis is implemented with a rim measurement of the main reflector. The origin and details of the measurement is unknown and exists as a text file, gbt_rim_v1.txt. The feed arm structure, consisting of circular struts, is included in the model but not used in analysis, a license with additional capabilities is required. The second model is derived from GBT Memo 155 where the sub reflector rim is analytic with equations input from a Mathematica notebook, Files: EM Modeling.4. The third model introduces a perfect conducting triangular plate for the feed arm and rectangular plate for the sub reflector support.

In comparing the AMD model with the GBT 155 generated version, there are slight differences in the sub reflector dimensions and axis angle that are a result of GRASP limitations for constructing surfaces. An upgraded version of GRASP, 25.1, added a feature for analytic rim construction that allowed a more intuitive approach. Adding the feed arm and sub reflector support increases the gain by few hundreds of dBs with the spill over remaining unchanged. It is worth noting that the GRASP treats the illumination of the surfaces as independent reflectors where the currents and corresponding far fields are added potentially giving nonphysical results for efficiency. For this reason, the sub reflector support could not extend over the sub reflector.

An analysis with an idealized Gaussian feed with taper angle 15 degrees and edge taper set to14.2 dB is compared to a HE11 mode horn to show the differences. The results are shown in Table 2 (top, middle). The CST far fields were exported with origin set at the calculated phase center for the frequency 1.2 GHz, corresponding to the mounting ring position, see reference 3. GRASP includes a function that calculates the phase center for the imported tabular feed pattern. This routine is executed at each feed pattern frequency, shown in Table 2 (bottom), but not applied as a correction. The GRASP AMD and Klahold model phase center calculations do not coincide and are also different from the CST calculation.

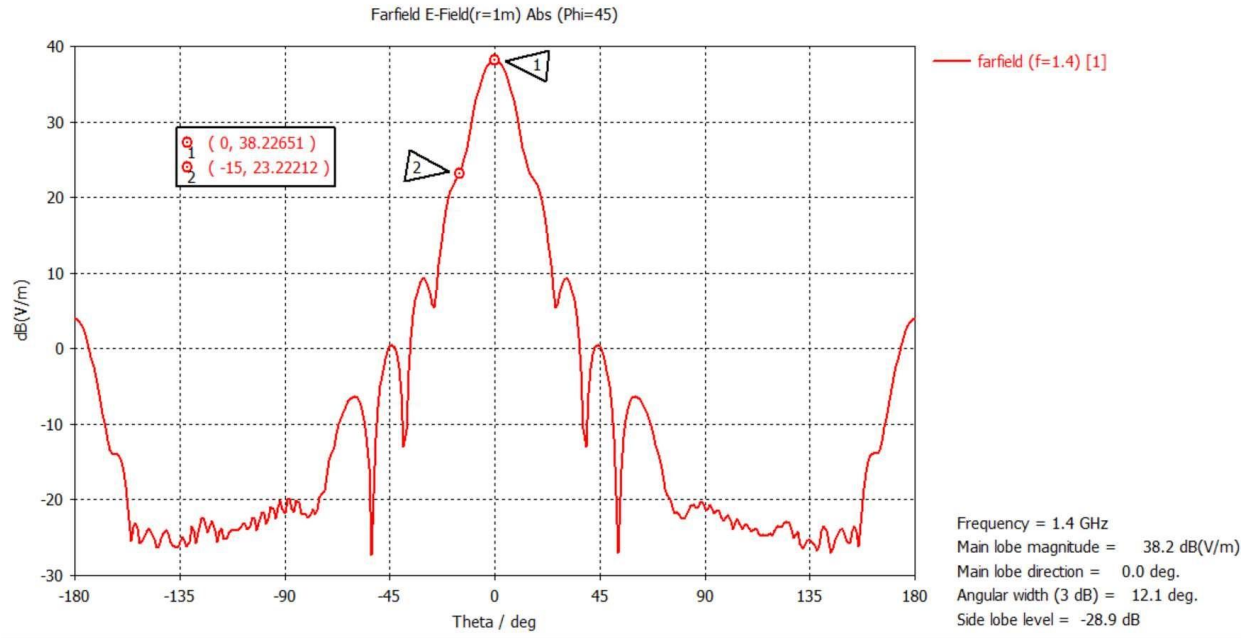

Figure 8. CST far field result at 1.4 GHz 45 degree cut illustrating 15 dB taper.

Aperture Center Location (Z, Y, X): (1632.584, 154.083, 183.437)

Phase Center [mm]

	Port 1: XL			Port 2: YR		
[GHZ]	Z	Y	X	Z	Y	X
1	656.546	151.817	183.487	657.499	154.138	185.947
1.1	539.115	154.135	183.437	539.070	154.088	183.381
1.2*	496.981	154.108	183.435	497.009	154.089	183.411
1.3	407.989	154.096	183.438	407.918	154.077	183.41
1.4	300.704	154.112	183.437	300.723	154.079	183.37
1.5	279.144	153.856	183.441	279.209	154.07	183.42
1.6	232.64	153.995	183.421	232.576	154.074	183.43
1.7	249.758	154.754	183.403	250.032	154.073	182.81
1.8	210.721	154.407	183.505	210.673	154.108	210.67
1.9	61.7979	156.735	183.483	61.4651	154.169	180.22
2	23.2404	150.179	183.506	23.1352	154.092	187.77

Table 1. CST far field phase center location. From measurements at frequency 1.2* GHz the phase center corresponds to the mounting ring and is used for GRASP export.

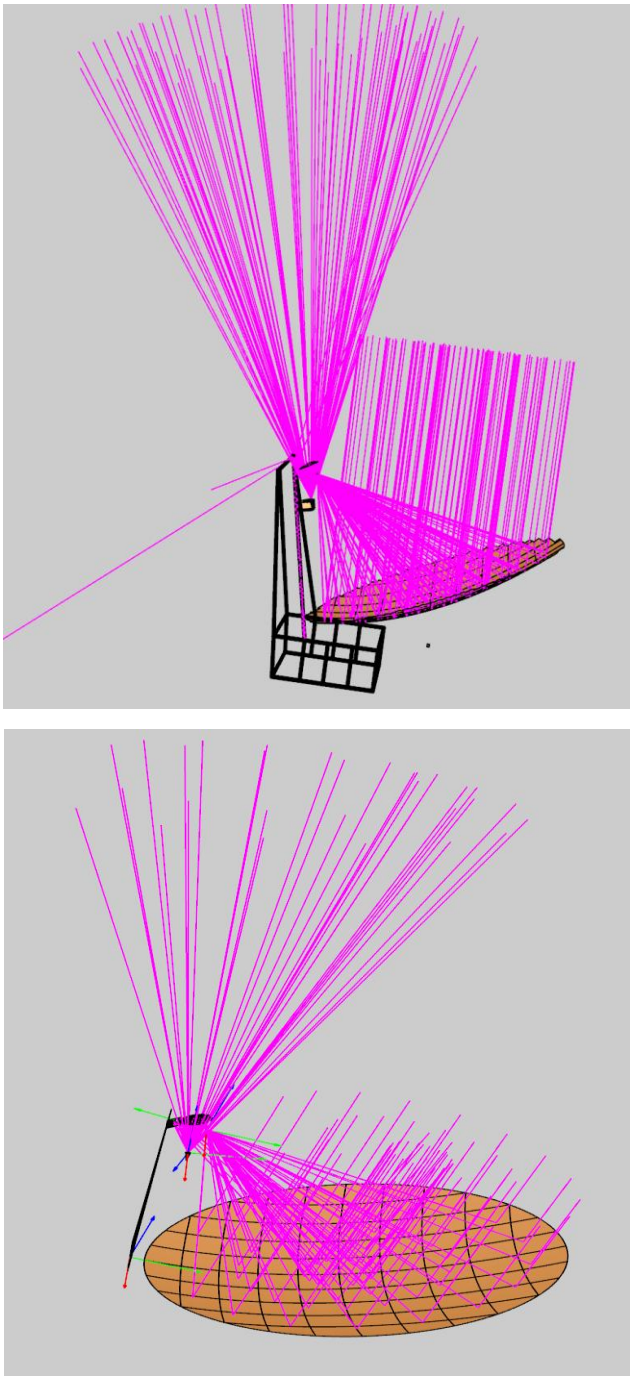

Figure 9. TICRA/GRASP models, AMD (Raytheon) top, GBT Memo 155 (Klahold) bottom, with the ray trace shown for a feed located at the Gregorian focus. The ray trace is not capturing the subtle differences between the idealized feed and the CST generated pattern. Both models show ray traces at half angle 23, corresponding to the -15 dB taper of Figure 8. These exceed the half angle of the sub reflector, 14.99 degrees.

GRASP Results Ideal Gaussian Beam								
[GHz]	Gain	η gain	η sub	T_{sub} [°K]	η main	T_{main}[°K]	T_{sys}[°K]	T_{sys}/η
1.0	59.15	0.749	0.959	0.285	0.943	4.78	33.57	44.83
1.1	59.98	0.749	0.959	0.266	0.945	4.40	28.20	37.64
1.2	60.75	0.751	0.960	0.245	0.946	4.11	20.23	26.92
1.3	61.44	0.751	0.960	0.235	0.947	3.86	17.83	23.75
1.4	62.09	0.752	0.960	0.228	0.948	3.65	16.89	22.47
1.5	62.70	0.754	0.961	0.216	0.949	3.47	16.24	21.55
1.6	63.26	0.754	0.961	0.212	0.950	3.31	17.03	22.61
1.7	63.79	0.754	0.961	0.208	0.950	3.17	17.91	23.75
1.8	64.30	0.756	0.961	0.205	0.951	3.05	19.30	25.51
1.9	64.77	0.756	0.961	0.203	0.951	2.94	22.20	29.35
2.0	65.21	0.756	0.961	0.201	0.952	2.84	28.08	37.17

GRASP AMD Model Results CST Far Fields GBT HE_{11} Horn (Figure 8)								
[GHz]	Gain	η gain	η sub	$T_{sub[^{\circ}K]}$	η main	$T_{main[^{\circ}K]}$	$T_{sys[^{\circ}K]}$	T_{sys}/η
1.0	58.59	0.658	0.880	0.83	0.865	4.78	34.12	51.86
1.1	59.44	0.661	0.881	0.77	0.868	4.37	28.70	43.40
1.2	60.21	0.664	0.892	0.66	0.870	4.10	20.65	31.09
1.3	60.93	0.667	0.884	0.68	0.872	3.90	18.35	27.50
1.4	61.59	0.669	0.884	0.66	0.872	3.63	17.32	25.88
1.5	62.20	0.672	0.885	0.64	0.875	3.43	16.66	24.81
1.6	62.77	0.674	0.886	0.62	0.876	3.22	17.37	25.79
1.7	63.31	0.675	0.887	0.60	0.877	3.09	18.24	27.01
1.8	63.82	0.677	0.887	0.59	0.878	3.02	19.69	29.07
1.9	64.30	0.679	0.888	0.58	0.879	2.89	22.52	33.18
2.0	64.75	0.680	0.888	0.58	0.880	2.82	28.46	41.86

GRASP AMD Model Phase Center Tabulated Feed	
[GHz]	GRASP Z [m]
1.0	0.772
1.1	0.624
1.2	0.437
1.3	0.200
1.4	0.077
1.5	-0.263
1.6	-0.449
1.7	-0.754
1.8	-0.778
1.9	-0.804
2.0	-1.111

Table 2. GRASP efficiency and spill over results for the ideal Gaussian illumination (above), for the GBT L band horn (middle), and the GRASP phase center calculation(bottom) for the Z coordinate, X and Y are ~ 0. Files: Excel.3. The correction for each frequency is not applied. Of note is the GRASP calculated phase center is an additional correction from the CST far field origin.

GRASP Klahold model Results CST Far Fields GBT HE_{11} Horn (Figure 8)								
[GHz]	Gain	η gain	η sub	T sub[°K]	η main	Tmain[°K]	Tsys[°K]	Tsys/ η
1.0	58.79	0.689	0.880	0.72	0.865	5.75	35.09	50.91
1.1	59.56	0.680	0.881	0.71	0.868	4.51	28.84	42.40
1.2	60.21	0.664	0.882	0.65	0.870	3.99	20.60	31.03
1.3	60.87	0.658	0.880	0.70	0.872	4.29	18.76	28.50
1.4	61.50	0.656	0.898	0.69	0.872	4.17	17.79	27.10
1.5	62.10	0.656	0.894	0.69	0.875	5.17	18.35	27.96
1.6	62.56	0.641	0.917	0.68	0.876	4.84	18.82	29.35
1.7	63.28	0.671	0.920	0.68	0.877	4.56	19.54	29.14
1.8	63.89	0.688	0.939	0.68	0.878	3.43	19.82	28.79
1.9	64.17	0.659	0.959	0.67	0.879	2.17	21.43	32.52
2.0	64.35	0.620	0.947	0.28	0.940	2.16	27.50	44.36
Phase Correction Applied								
[GHz]	Gain	η gain	η sub	T sub[°K]	η main	Tmain[°K]	Tsys[°K]	Tsys/ η
1.0	58.64	0.666	0.879	0.84	0.863	5.27	34.61	52.01
1.1	59.33	0.645	0.888	0.72	0.877	3.62	27.90	43.24
1.2	60.11	0.649	0.888	0.69	0.877	3.49	20.06	30.92
1.3	60.83	0.652	0.883	0.69	0.871	4.13	18.58	28.51
1.4	61.47	0.652	0.898	0.58	0.886	4.15	17.76	27.24
1.5	62.13	0.661	0.986	0.08	0.880	5.09	17.77	26.88
1.6	62.68	0.659	0.924	0.41	0.911	4.06	18.00	27.31
1.7	63.32	0.677	0.923	0.41	0.910	4.31	19.26	28.47
1.8	63.90	0.690	0.941	0.31	0.931	3.26	19.64	28.48
1.9	64.25	0.671	0.962	0.20	0.956	2.09	21.34	31.79
2.0	64.54	0.647	0.950	0.26	0.945	1.77	27.09	41.84

GRASP Klahold Model Phase Center Tabulated Feed	
[GHz]	GRASP Z [m]
1.0	-0.205
1.1	-0.482
1.2	-0.359
1.3	-0.141
1.4	-0.274
1.5	-0.077
1.6	-0.307
1.7	-0.149
1.8	-0.123
1.9	-0.333
2.0	-0.428

Table 3. GRASP Klahold model efficiency and spill over results for the GBT L band horn (top) Files: Excel.1. This model includes the effects of the feed arm and prime focus boom. The phase center correction (right) was applied for comparison in the table (bottom). A phase center correction is not possible in the Gaussian pattern, both the AMD and Klahold model give similar results.

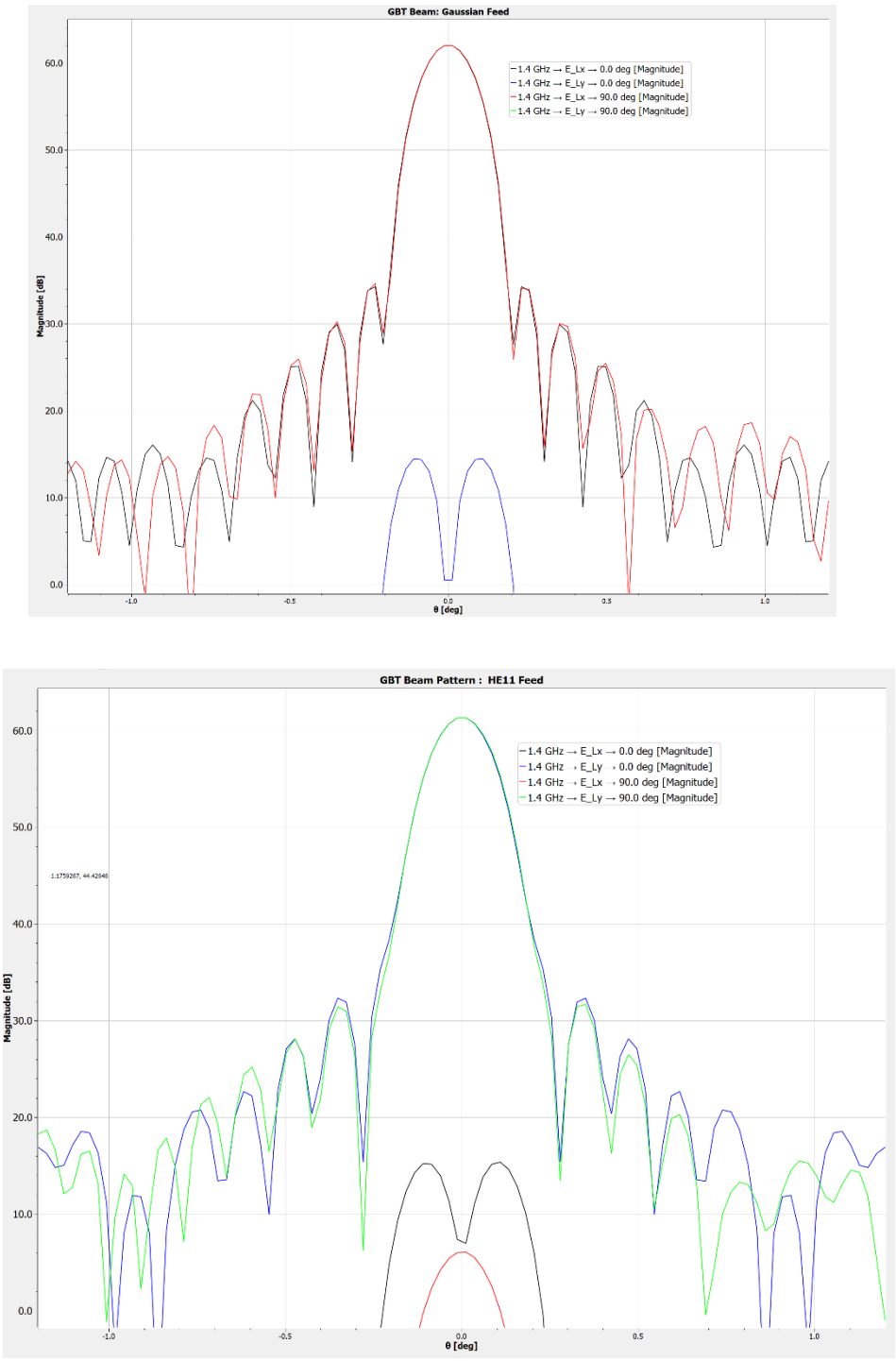

Figure 10. GBT L-band Beam: TICRA/GRASP model comparing an ideal Gaussian illumination (above) and the GBT L band horn illumination (below). The cross polarization in the GBT L band illumination is indicative of an asymmetrical illumination from the CST model far fields.

GBT SEFD Measurements

A metric to gauge the accuracies of the physical optics model is calculated with GBT system equivalent flux density, SEFD, observations, Figure 11. These measure the GBT response from known flux calibration sources. An on "On" source observation is followed by an identical cold sky, or "Off" source observation. The ratio of "Off" source to "On" minus "Off" is scaled by the known flux value giving SEFD in Jansky's. When scaled by the factor 2.845 K/Jy (Appendix III), the result is a direct measure of system temperature divided by the total efficiency. To compare the GRASP model total efficiency and spill over predictions are required. The spill over noise temperature is added to the estimated receiver temperature contribution at the feed aperture, CMD background, and atmospheric model contribution to comprise a total system temperature.

Evan Smith provided a description of the observations as follows: the data was collected by splitting the full L-band frequency range into 5 IF windows. The window size was 187.5 MHz, with 32768 channels with 10% overlap, and center frequencies of 1143.75, 1312.5, 1481.25, 1650, and 1818.75 MHz. The project ID is TGBT25B_608 and the sessions are 04, 18, and 20, taken August 27, September 20th, and October 9th, 2025, respectively. The scans were 60-second position-switched with noise calibration. The band is split into 5 IF windows to protect the full bandwidth against unbalancing due to heavy RFI from GPS, Iridium, and CARSR Radar. The flux calibration sources are non-standard, ranging from 1-2 Jy, as opposed to standard calibration sources (>15 Jy) that can cause balancing issues between the "On" and "Off" source positions. Known polynomial fluxes were generated using information from the VLA calibrator catalogue. The frequency-dependent data for each window in succession (with no consideration for the overlap) was stored with one out of every ten frequency/SEFD values saved.

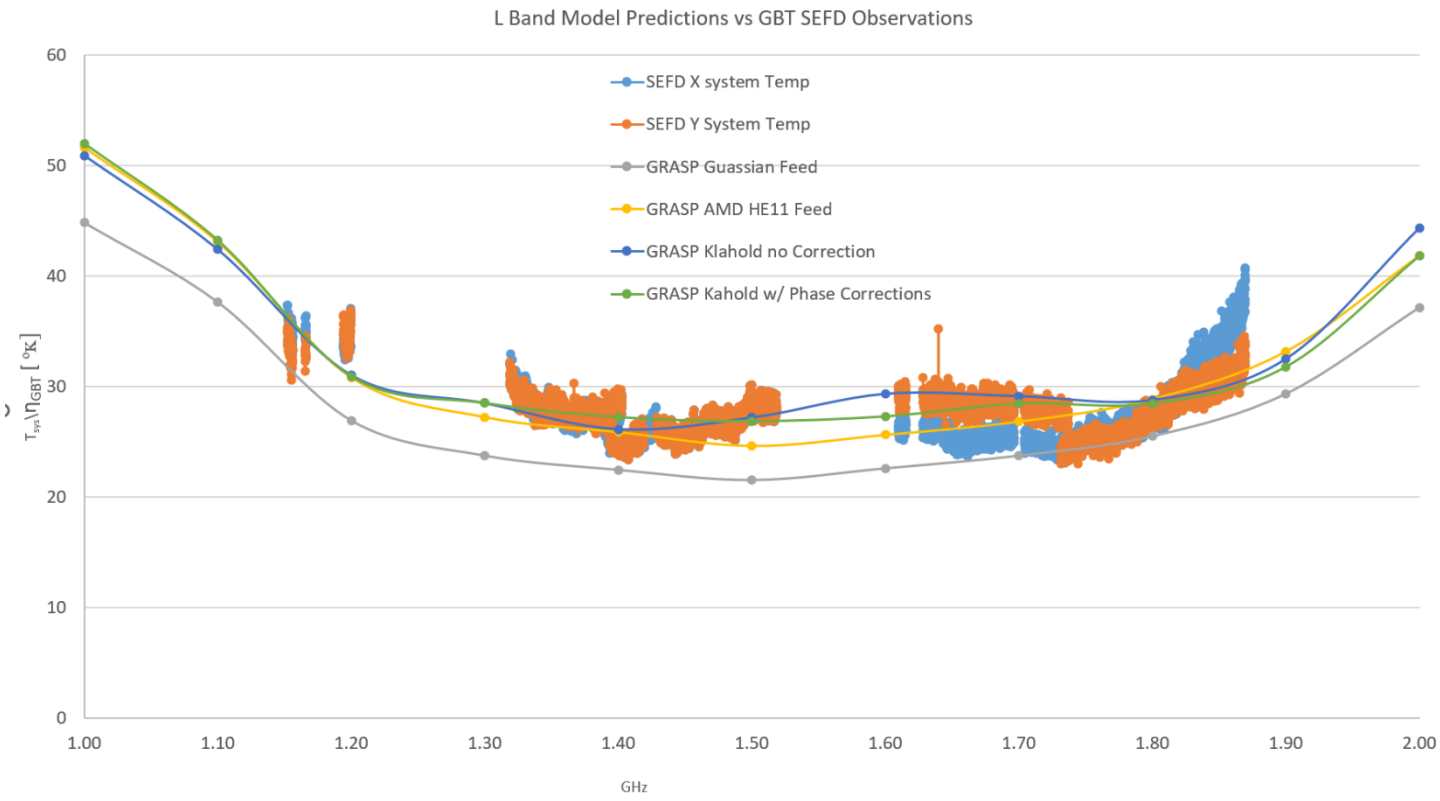

Figure 11. $\frac{T_{sys}}{\eta}$ predictions based on GRASP GBT AMD and the Klahold model where the noise contributions are shown in Table 4. The SEFD observations of VLA calibrator sources 0632+103,1227+365, and 1800+7828 are converted to temperature from Janky's with the multiplier 2.845 ºK/Jy, Appendix II. The Gaussian feed gives nearly identical predictions (gray curve) in both models; however, the AMD model (yellow curve) predicts better performance for the frequency range 1.2 to 1.8 GHz. The Klahold model with phase corrections from Table 3 shows some improvement in phase efficiency when applied at the 100 MHz frequency spacing (green curve).

GHz	$T_{sub[^{\circ}K]}$	$T_{main[^{\circ}K]}$	T_{LNA}	T_{rvr}	$T_{cmb,atm}$	T_{sys}	T_{sys}/η
1.000	0.285	4.780	12.553	21.553	8.180	33.57	44.83
1.100	0.266	4.373	8.417	17.080	6.572	28.20	37.64
1.200	0.245	4.102	6.044	9.750	5.551	20.23	26.92
1.300	0.235	3.831	5.087	7.880	4.868	17.83	23.75
1.400	0.228	3.628	4.862	7.340	4.392	16.89	22.47
1.500	0.216	3.426	4.659	7.050	4.049	16.24	21.55
1.600	0.212	3.291	4.439	8.100	3.796	17.03	22.61
1.700	0.208	3.155	4.359	9.210	3.604	17.91	23.75
1.800	0.205	3.020	4.807	10.807	3.455	19.30	25.51
1.900	0.203	2.953	6.845	13.845	3.339	22.20	29.35
2.000	0.201	2.818	11.912	19.912	3.246	28.08	37.17

Table 4. GRASP AMD model $\frac{T_{sys}}{\eta}$ temperature components used in Figure 11 for the GBT L band HE11 horn. The measured LNA noise temperatures are included in total measured receiver noise temperature referenced to the feed aperture. The total system temperature values then combines the receiver, spill over, atmospheric and CMD contributions (see Files: Excel.3 for details), $T_{sys} = + T_{main} + T_{sub} + T_{rvr} + T_{cmb,\,atm}$.

Noise Temperature and Calibration Measurement

The receiver noise temperature was measured with test configuration that consisted of the NRAO Liquid Nitrogen calibrated load, serial number SN LN4, load for both hot and cold load. This is connected to the coaxial input of a WR650 transition that is followed by a step impedance circular to rectangle transition as shown in Figure 12. The measurements verified calibration values are consistent with the 2005 and 2002 measurements. However, the models and measurement of the test fixtures proved to be inaccurate giving measurement variance and variability on the order of the low power noise diode calibration values. Since the hot and cold load injection is polarized by the coaxial-to-waveguide transition, and thus correlated, the circular polarization calibration cannot be measured. There is doubt on the value of circular polarized calibration given the injection is not phased for a particular polarization, neither left, or right.

Figure 12. Noise Temperature LN_2 Test. The serial number LN04 connected to the coaxial to WR650, followed by the stepped impedance WR650 to circular transition. The output of the receiver is mixed down to a final bandwidth of 50 MHz and detected with the Agilent E4418 power meter.

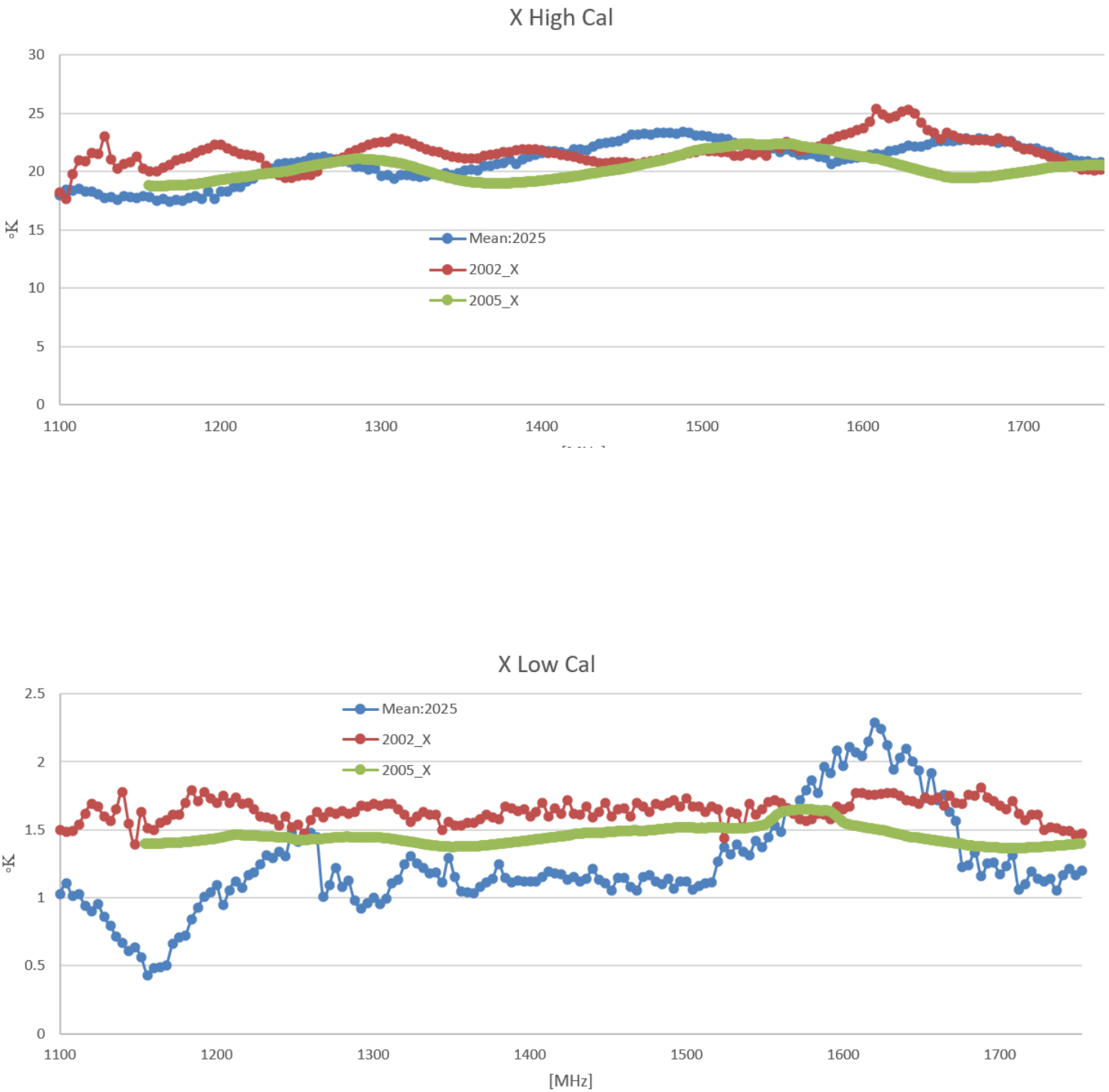

Figure 13. Measured X calibration high (top) and low calibration (bottom)
The high calibration values show much lower deviation from previous determinations, 2005 (sky), 2002 (Indoor Outdoor with feed).

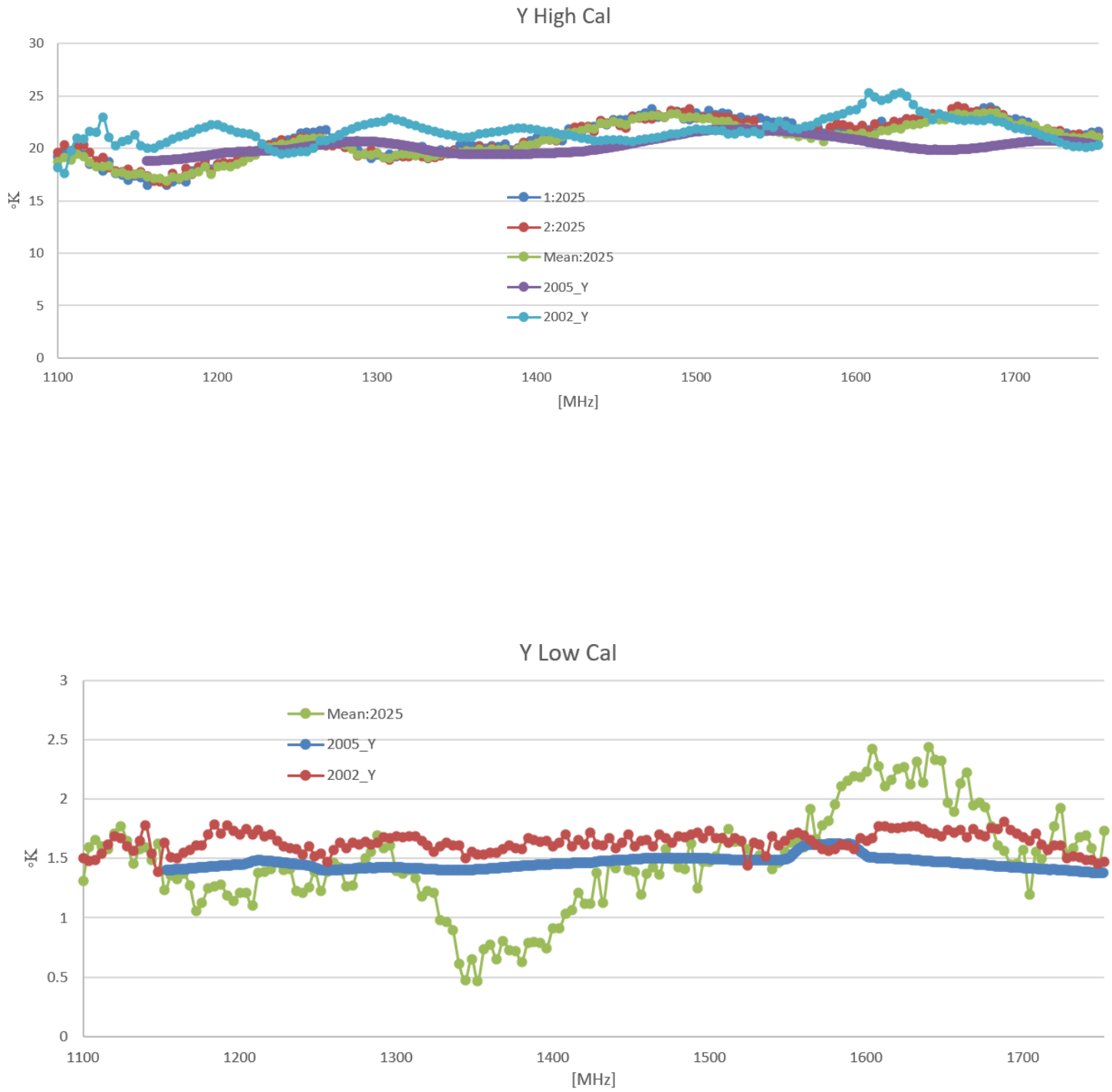

Figure 14. Measured Y calibration high (top) and low calibration (bottom)
The high calibration values show much lower deviation from previous determinations, 2005 (sky), 2002 (Indoor Outdoor with feed).

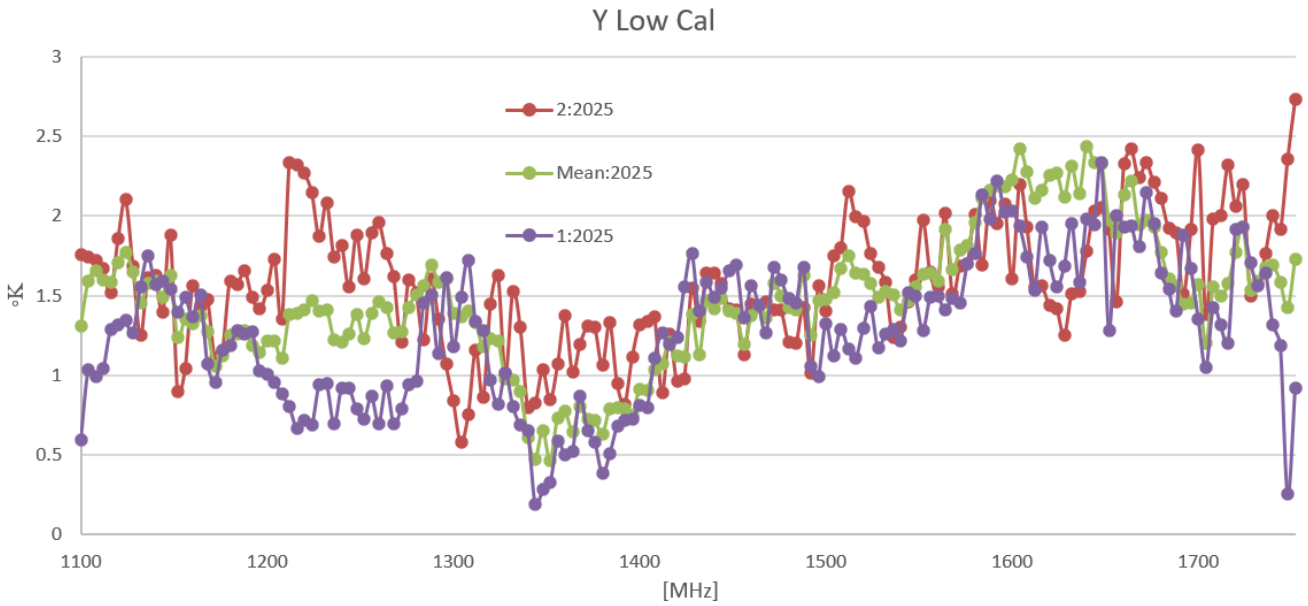

Figure 15. The Y low calibration measurement variability in each compared to the mean.

LNA Bias Cards

The LNA bias cards shown below are designed with circuitry that allows adjustment of the last stage current, I_D. This can be adjusted in the CLEO manager as shown below, in this case X is 3, and Y is -4. The values refer to the voltage input with range of -10 to +10 Volts. The scale is not calibrated but effectively changes the set point of the last stage current, which in turn affects the overall gain and compression point without significantly altering the noise temperature. The adjustment is input on pin 20 of the edge connector, shown on the left. The top card, Y channel, has the feature; however, the bottom view shows a card without the connection, X channel. Also, the ability to turn the bias off is dependent upon the card build. The top view, left, shows the relay that removes the bias voltage. The bottom card has the relay removed and is without the functionality.

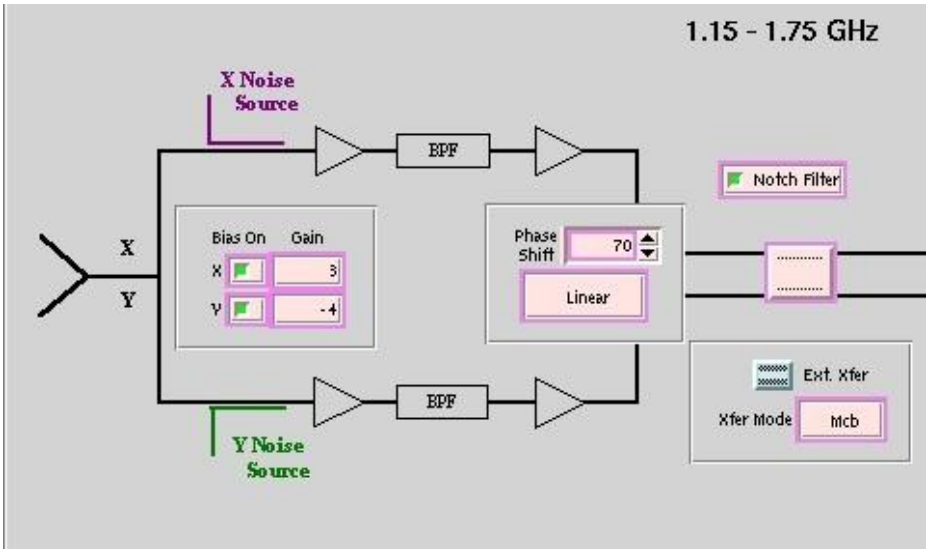

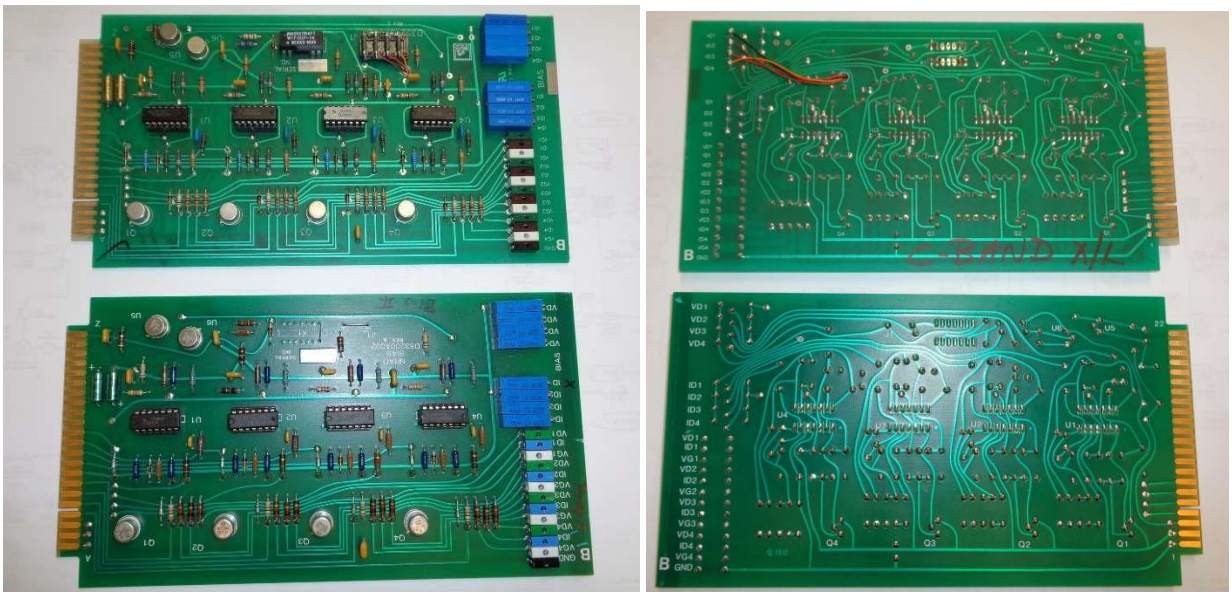

Figure 16. CLEO manager snapshot showing the gain control and “off” features. Two versions of the bias card. The top has the functionality; the bottom card does not the circuitry or components.

LNA Noise Temperature Measurement

All the available L-band low noise amplifiers were tested cryogenically for noise temperature and S parameters. These are compared with the available data from CDL.[5] The measurements in Figure 17 agree with the data from reference number four. The measurement technique and calibration are described in detail EDTN 23.[1]

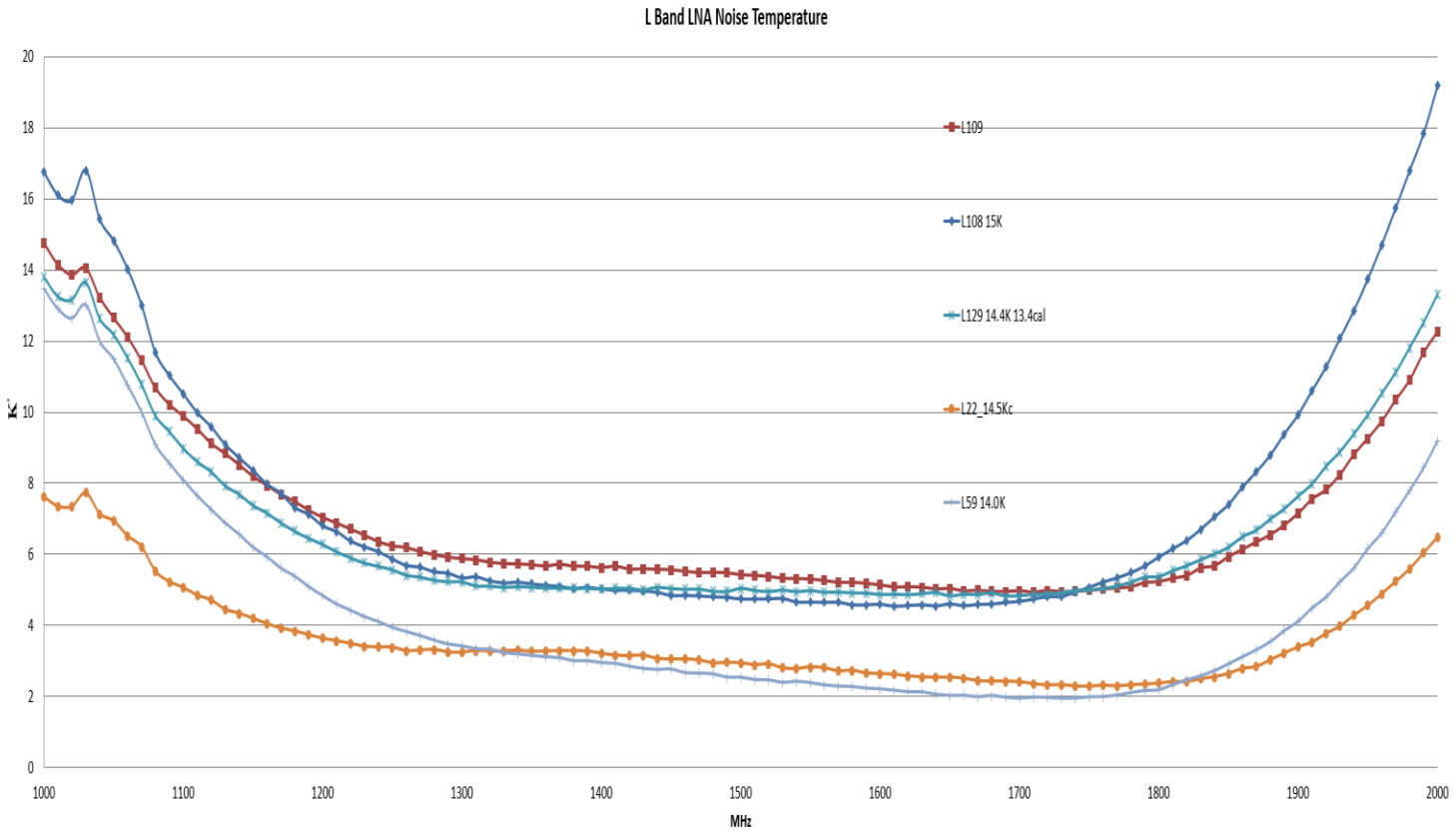

Figure 17. Noise temperature measurement plot from Files EXCEL: 1. Serial Numbers L109, L108, L129, L22, L59.

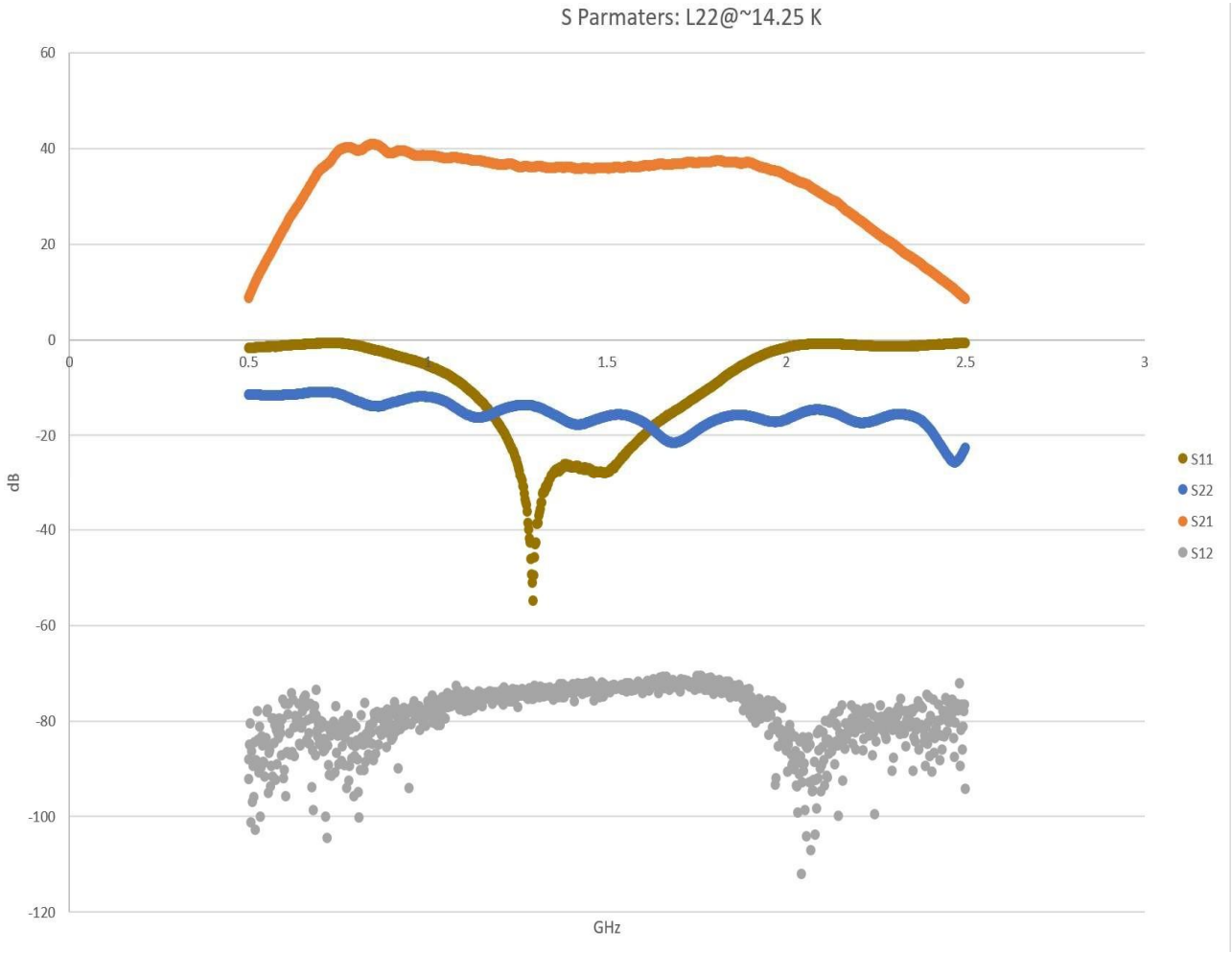

Figure 18. Example VNA measurement plot from Files EXCEL: 2.

S-band Noise Calibration Measurement

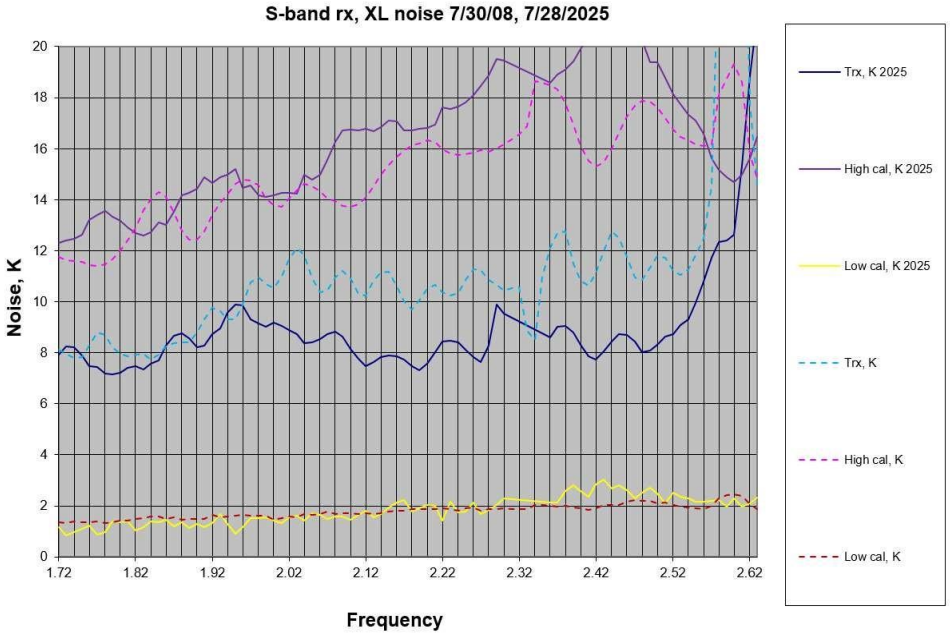

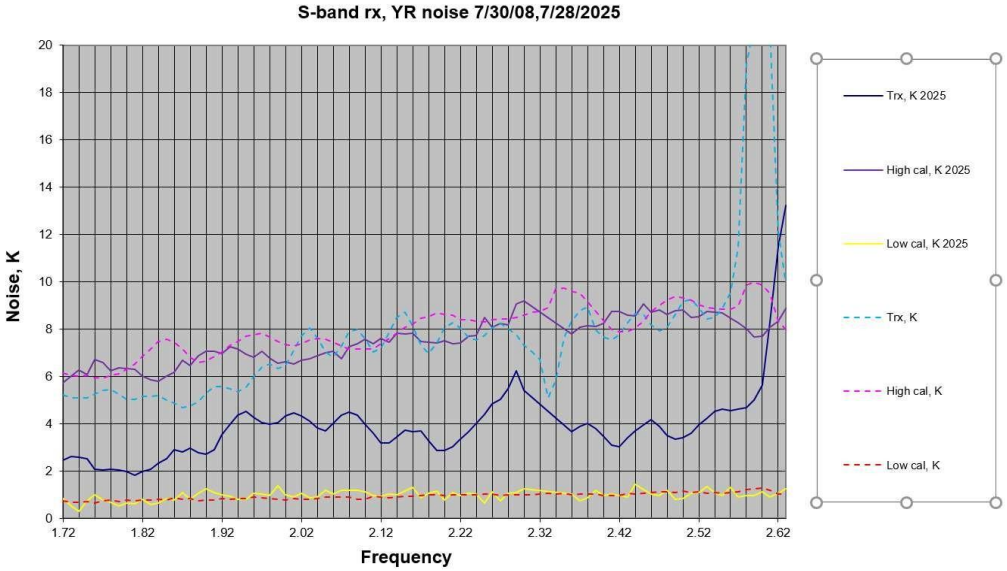

Figure 19. S band noise temperature and calibration amplitudes for channel XL (above), and YR (below). The measurement is identical to the L-band technique described in the "Noise Temperature and Calibration Measurement" section and shown in Figure 12.

Files:Excel

Path: gbfiler\doc\drawings\Archive\GBO Electronics\35242, L-band rx, 1.15-1.73 ghz\		
	File	Description
1	documentation\LNA Data\Lband_LNA_NoiseTempMeas.xlsm	Test Dewar Noise Temperature
2	documentation\LNA Data\VNA_Lband_LNA_Sparameters.xlsm	S parameter data (source of Figure 2)
3	Lband_Tsys_wGrasp.xlsm	GRASP Tsys/Noise analysis of Table 2.
4	35242, L-band rx, 1.15-1.73 ghz.xls	Drawing number list.

Files:EM modeling

1	Gbfiller\doc\Archive\GBO Electronics\35242, L-band rx, 1.15-1.73 ghz\documentation\	Description
2	TICRA_GRASP\gbt_nrao_AMD_Rev5_20230816_SDW_Lband	GRASP model of GBT Gregorian Focus: ”Array Main Dish”.
3	TICRA_GRASP\L_band Klahold Model\L_band_GREG	GRASP model derived from GBT Memo 155.
4	TICRA_GRASP\ SDW_ellipsoid_xy_projection.nb	Mathematica notebook that generates equations for ellipsoid analytical rim
5	\CST\Feed_repair	Feed and OMT combination for all the GRASP export FF files.
6	\CST\Ltrans	Coax to WR-640 transition
7	\CST\Ltrans_cir_rec	Circular to WR-640 Transition
8	\CST\OMT_all	OMT all modes (polarization)

Photographs

Path: gbfiler\doc\drawings\Archive\GBO Electronics\35242, L-band rx, 1.15-1.73 ghz\documentation\pics		
	File	Description
1	Feed_LAB_VNA_Absorber.jpg	Testing Feed Assembly Absorber close up.
2	Feed_LAB_VNA_Hoist.jpg	Testing Feed Assembly Hoist close up.
3	Feed_LAB_VNA_Strap.jpg	Testing Feed Assembly Strap close up.
4	\Test Fixtures\Circular_Offset_L11p93.JPG	Circular Offset length 11.93 inches.
5	\Test Fixtures\Circular_Offsets.JPG	Circular Offsets for calibration.
6	\Test Fixtures\Circular_Rec_Step_Trans.JPG	Circular to Rectangular Transition stepped impedance.
7	\Test Fixtures\Circular_Rec_Step_Trans_Top.JPG	Circular to Rectangular Transition stepped impedance top view.
8	\Test Fixtures\ShortingPlate.JPG	Shorting Plate
9	\Test Fixtures\SinglePol_load.JPG	Single polarization sliding load.
10	\Test Fixtures\SinglePol_load_2.JPG	Single polarization sliding load.
11	\Test Fixtures\SlidingLoad_CO1p04437_top.JPG	Sliding load cutoff frequency 1.04437 GHz.
12	\Test Fixtures\SlidingLoad_CO1p04437.JPG	Sliding load cutoff frequency 1.04437 GHz.
13	\Test Fixtures\SlidingLoad_CO1p076.JPG	Sliding load cutoff frequency 1.076 GHz.
14	\Test Fixtures\Zeeman_trans.JPG	Transition for L band circular waveguide to Zeeman feed.
15	\Test Fixtures\Bias Card Front.JPG	Front view of the LNA bias cards.
16	\Test Fixtures\Bias Card.JPG	Rear view of the LNA bias cards.
17	\Test Fixtures\LN2 NT setup.JPG	Noise Temperature Measurement Tests Configuration.

Appendix I

(credit: Walter Klahold Mathematica Notebook)

Deriving the rim analytical equation for the sub reflector deserves further explanation. Although complicated, this method is a more logical approach than attempting to manipulate the available parameters for the GRASP ellipsoid. This method can also be employed to define other surfaces.

GBT Memo 155 parameters.

α: 17.899˚, angle from the ellipsoid axis, secondary focus, to the center of the sub reflector.
θ_H: 14.99˚, half angle of the opening angle of the sub reflector.
a: 10.417m, major semi axis of the sub reflector parent ellipsoid.
C: 11m, distance between ellipsoid foci.
e: 0.528, eccentricity of the sub reflector parent ellipsoid.

With these parameters one can derive the rim coordinates that intersect with the cone of angle, θ_H, with vertex located at the Gregorian focus. One simplification of this approach from the GRASP ellipsoid definition is the position of the coordinate system. GRASP default is the center of the ellipsoid, whereas the GBT coordinate system is defined at the primary focus. Translating the coordinate system and properly defining the sub reflector dimensions is cumbersome when using the default.

The vector approach for the cone representation begins by defining a unit vector, n_0, located at the secondary focus that is aligned with the feed axis. A second unit vector, n_1, also located at the secondary focus and pointed at the upper edge of the sub reflector. A third unit vector, n_2, is then defined by transforming n_1 with rotation matrix, R, about vector n_0. A free parameter, u, defines the angle of rotation. Since the unit vectors are defined from the secondary focus and are of unit length, a vector, $\overrightarrow{p(u)} = t * \mathrm{n2}$, is defined and is the resultant vector from the ellipsoid coordinate origin. The resultant is derived from a fixed vector from the ellipsoid origin to the secondary focus with a scaled version of the rotated vector, n_2. The scale factor parameter, t, varies as the parameter u ranges from 0 to 2π. The expression for $\overrightarrow{p(u)}$ is solved with the equation of the sub reflector ellipsoid to obtain the analytic expression for the rim referenced to the primary focus point. The solutions give expressions for the coordinates x, y, z, and t. One extraneous solution represents the intersection on the primary reflector side of the prime focus. GRASP does not require the t solution. The solutions for the analytical rim are:

$$x = \frac{49.296 \sin(u)}{-12.262 + \cos(u)}$$

$$y = \frac{16.897 - 14.008 \cos(u)}{-3.899 + 0.318 \cos(u)}$$

$$z = -19.729 + \frac{1}{0.0362 - 0.00295 \cos(u)}$$

$$t = \frac{1}{0.0685 - 0.00559 \cos(u)}$$

Position vector: $\overrightarrow{p(u)} = t\,\overrightarrow{n_2(u)} - \left(0,0,-\frac{C}{2}\right)$

Rotation matrix:

$$\begin{pmatrix} \mathrm{n}_{2x}(u) \\ \mathrm{n}_{2y}(u) \\ \mathrm{n}_{2z}(u) \end{pmatrix} = \begin{pmatrix} Cos[u] & -Cos[\alpha]\,Sin[u] & -Sin[\alpha]\,Sin[u] \\ Cos[\alpha]\,Sin[u] & Cos[u] + (1 - Cos[u])\,Sin[\alpha]\text{^}2 & -Cos[\alpha]\,(1 - Cos[u])\,Sin[\alpha] \\ Sin[\alpha]\,Sin[u] & -Cos[\alpha]\,(1 - Cos[u])\,Sin[\alpha] & Cos[\alpha]\text{^}2\,(1 - Cos[u]) + Cos[u] \end{pmatrix} \begin{pmatrix} \mathrm{n}_{1x} \\ \mathrm{n}_{1y} \\ \mathrm{n}_{1z} \end{pmatrix}$$

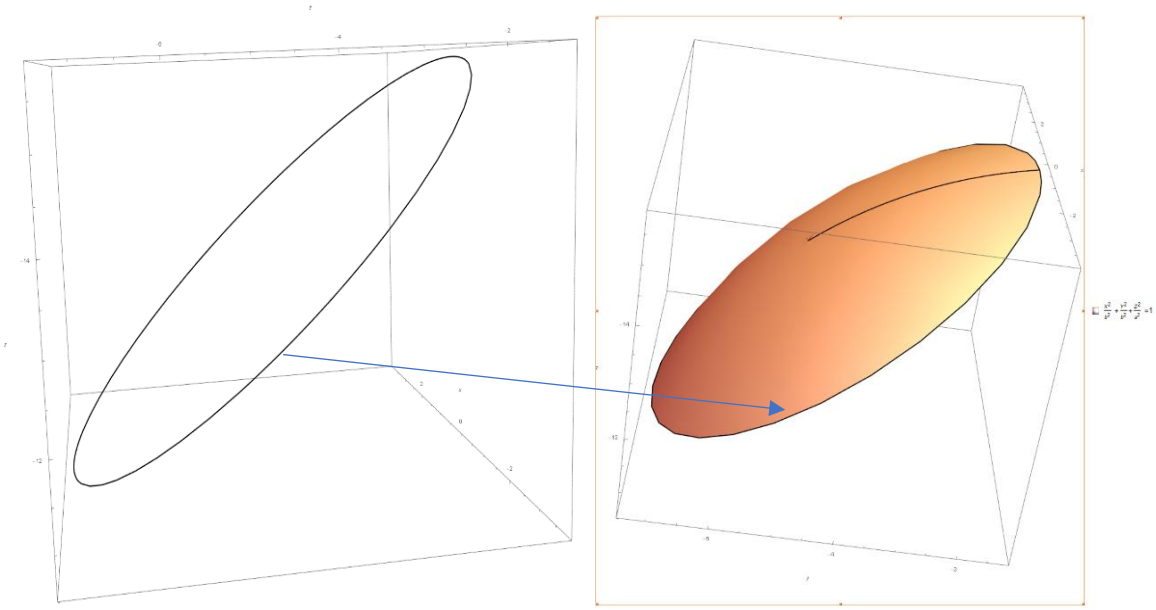

Parametric plot of the analytic rim equation, left, superimposed on the parent ellipsoid, right. The origin of the coordinate system is the parent ellipsoid center. The free parameter, u, ranges from 0 to 2π, left. To coincide with the GBT parent parabola coordinate system, i.e. focal point, the z coordinated requires a shift of – C/2. Also, for GRASP analysis the sub reflector is rotated by angle, β=-5.57, about the primary focus.

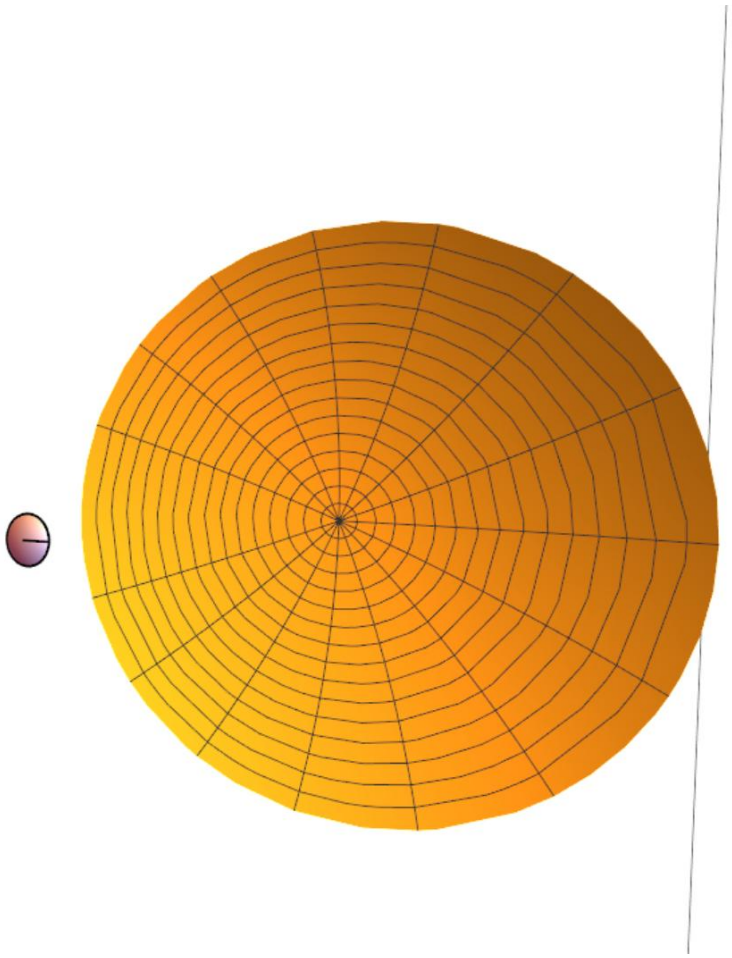

The described technique generates the primary reflector from the parent paraboloid equation $4\,f(f-z) = x^2 + y^2$, $f = 60$ *meters with the GBT coordinate system, shown with the sub reflector.*

θ^*: 39.005 half angle of the cone that intersects with the paraboloid to form the surface.
θ_0: 42.825 cone axis angle from the Z axis.

Appendix II : Atmospheric and Galaxy Temperatures

The atmospheric and galactic contributions are estimated by the weather predictions of absorption, atmospheric temperature (@2 GHz value), and galactic position (strongly frequency dependent) as:

$$T_{gal} = 22.3 \left(\frac{0.408}{\nu}\right)^{2.6}$$

T_{gal} depends upon the beam size and differs from the GBT measurements, but not significantly. The calculated temperature is based on the 60^{o} beam that incorporates > 90% of the power available.

$T = (T_{gal} + T_{CMB})\, e^{-\tau\, airmass} + T_{atm}\left(1 - e^{-\tau\, airmass}\right)$
T_{cmb} = 2.7
T_{atm}= 260, τ = 0.008, airmass = 1.0236 :
typical values taken from the weather reports at the time of measurement.[8]

Appendix III : SEFD Calculation

Defined (Wrobel & Walker)[7]

$$SEFD \stackrel{\text{def}}{=} \frac{\mathrm{T}_{sys}}{\mathrm{K}}$$

$$K_{GBT} = \frac{\eta\, A}{2k_b} \quad \text{(single polarization antenna performance)} \quad \frac{^\circ K}{\text{Jansky}}$$

$$P_{src} = g_{GBT}{}^2\, k_b\, K_{GBT}\, S_{src}\, \Delta\nu \quad \text{(received power)}$$

A known calibration source, S_{src} ,is observed producing a detected power, P_{src}, per polarization. The same consideration is applied to $P_{OFF}$where the total power is half the value when both polarizations are included. Since P_{ON} is per polarization, the factor of two is not included.

$$P_{OFF} = g_{GBT}{}^2\, k_b\, T_{sys}\, \Delta\nu \qquad \text{(system power no source)}$$

$$P_{ON} = g_{GBT}{}^2\, k_b\, T_{sys}\, \Delta\nu + g_{GBT}{}^2\, k_b\ K_{GBT} S_{src}\, \Delta\nu \quad \text{(system power with source)}$$

$$\frac{P_{OFF}}{(P_{ON} - P_{OFF})} = \frac{g_{GBT}{}^2\, k_b\, T_{sys}\, \Delta\nu}{g_{GBT}{}^2\, k_b \Delta\nu\ K_{GBT} S_{src}}$$

Substituting gives

$$\frac{P_{OFF}}{(P_{ON} - P_{OFF})} = \frac{T_{sys}}{(S_{src} K_{GBT})}$$

$$\frac{P_{OFF}\ S_{src}}{(P_{ON} - P_{OFF})} = \text{SEFD} \qquad [Jansky]$$

Substituting the proportional measured values C_{ON} and C_{OFF} for P_{ON} and $P_{OFF,}$ respectively

$$\frac{C_{OFF}\ S_{src}}{(C_{ON} - C_{OFF})} = \text{SEFD}$$

To convert the SEFD to temperature a unity gain definition is introduced:

$$K_e \stackrel{\text{def}}{\equiv} 1 \frac{^{\circ}K}{Jy}$$

Solving for an equivalent aperture size for SEFD =1 and η = 1 gives:

$$\eta \, \mathrm{A}_e = 2 \, k_b \, K_e = \frac{2 * 1.38065 \, 10^{-23}}{10^{-26}} = 2761 \text{ m}^2$$

and

$$\mathrm{A}_{GBT} = \pi \, r^2 = 7853.98 \text{ m}^2$$

$$\frac{K_{gbt}}{K_e} = \frac{\eta_{gbt} \, \mathrm{A}_{GBT}}{\mathrm{A}_e} = \frac{\eta_{gbt} \, 7853.98}{2761} = \eta_{gbt} \, 2.845 \; [\frac{^{\circ}\mathrm{K}}{\text{Jansky}}]$$

$$SEFD \, K_{gbt} = \frac{\mathrm{T}_{sys}}{\eta_{gbt}}$$

$$\left(\frac{C_{OFF} \; S_{src}}{(C_{ON} - C_{OFF})} * 2.845 \right) = \frac{\mathrm{T}_{sys}}{\eta_{gbt}}$$

References

1. White S., Leyzorek L., Simon R., EDTN 23 "Test Dewar Design".
2. Stennes, M. Test Data GBT L-Band from Binder. 1996.09.18

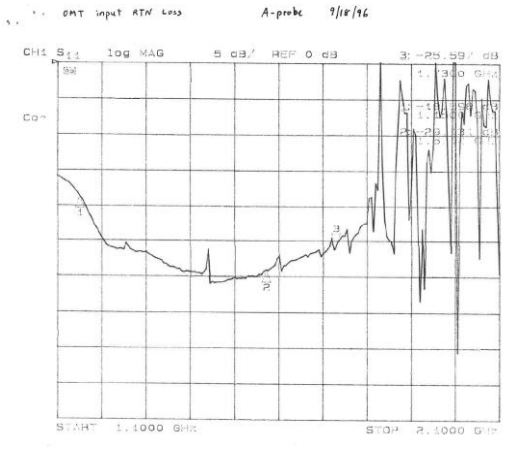

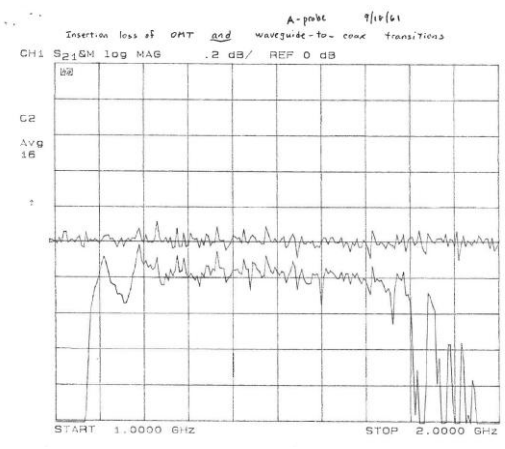

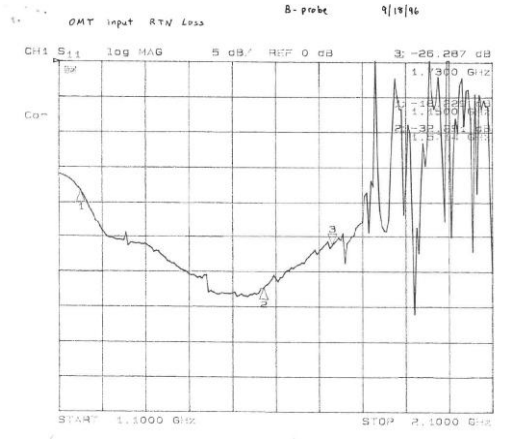

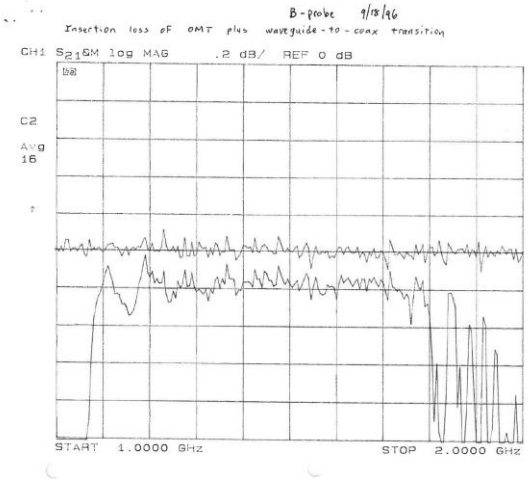

3. Srikanth, S. Test Data GBT L-Band Feed 1.15-1.73 GHz. 1996.11.05

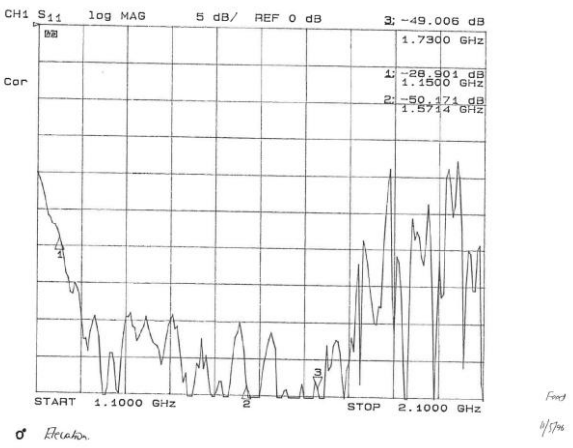

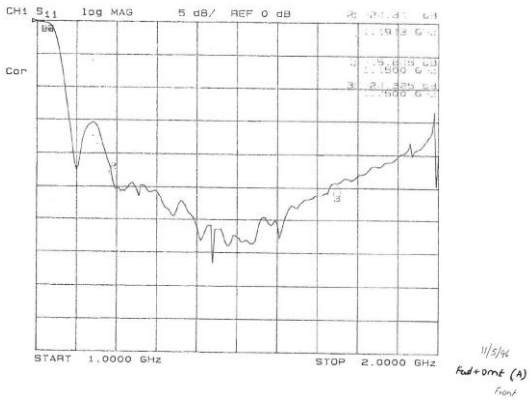

4. Srikanth, S. GBT L-Band Feed Memorandum. 1997.01.16

Input return loss of the feed was measured in November 1996. The feed was mounted on the ring at the indoor/outdoor test building at Green Bank. Return loss was measured at different elevation angles in order to check if there was any deflection of the feed. Measured results are shown in Figure 1. Return loss is better than -29 dB in the 1.15 to 1.73 GHz frequency range. Comparing the 0 and 60 degree elevation results, it is seen that a few reflection peaks are up by 3 dB at the most at 60 degree elevation. The stiffening provided by the fiber glass encasing seems sufficient.

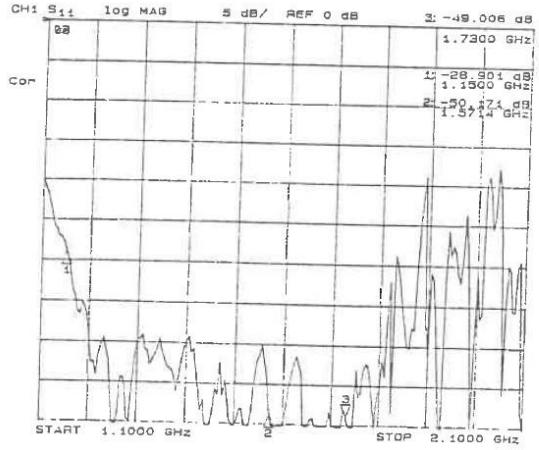

a) 0 degree elevation

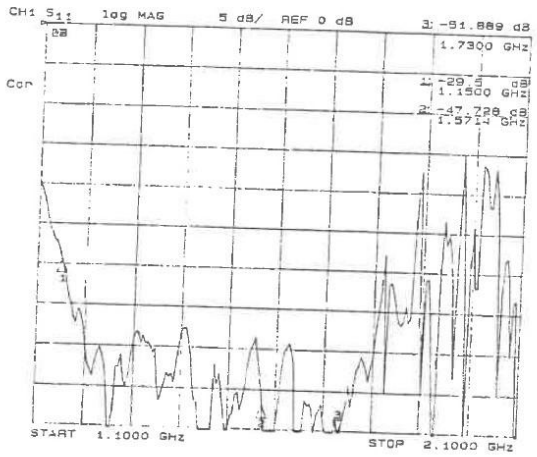

b) 30 degrees elevation

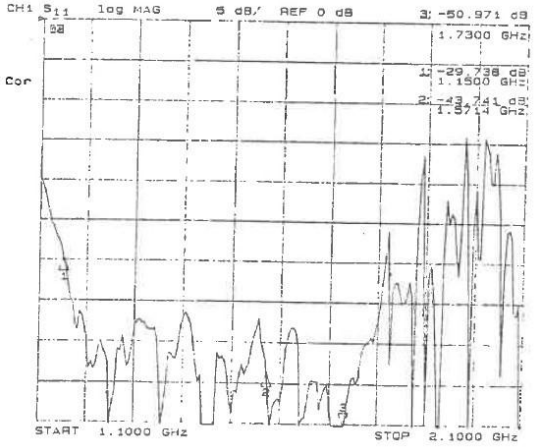

c) 45 degrees elevation

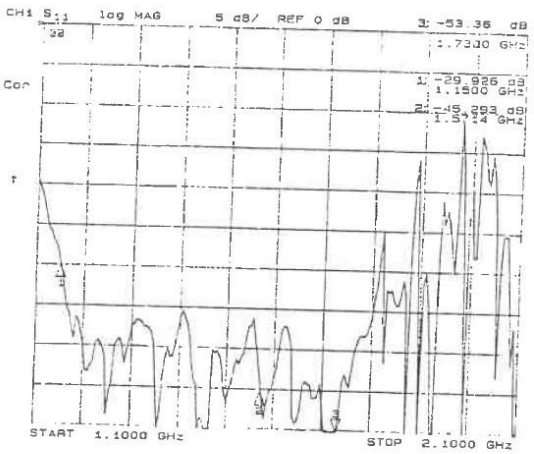

d) 60 degrees elevation

Figure 1. Measured input return loss

GBT L-Band Feed

Freq. (Ghz)	Taper at 15 deg. (dB) E	H	45deg.	Cross.Pol. (dB)	PC Location* (ins.)
1.00	-12.0	-12.5	-12.4	-30.5	
1.10	-13.8	-13.7	-13.4	-30.9	+17 5/8
1.15	-15.0	-14.2	-14.3	-34.0	
1.20	-14.5	-14.3	-14.0	-38.0	0
1.30	-13.9	-14.0	-13.9	-39.0	-7 11/16
1.40	-14.1	-14.0	-13.7	-36.5	
1,50	-13.7	-13.9	-13.8	-36.0	
1.60	-14.0	-15.5	-15.1	-27.5	-14 3/16
1.70	-13.9	-15.2	-14.8	-24.5	
1.73	-14.5	-15.0	-15.5	-25.5	
1.75	-15.0	-15.3	-15.0	-21.0	
1.80	-13.3	-15.0	-15.7	-21.0	

* Phase center location from the mounting ring surface
+ corresponds to location towards the feed aperture
- corresponds to location towards the feed throat.

5. Cvfiller\cv-cdl-pub\AmplifierTestData$\1.2_1.8_GHz network location of amplifier data.
6. https://alda.gb.nrao.edu/receiver/receivers/Rcvr1_2/ website where the calibration values can be downloaded (requires permission).
7. **Title:** Sensitivity
   Authors: Wrobel, J. M. & Walker, R. C.
   Journal: Synthesis Imaging in Radio Astronomy II, A Collection of Lectures from the Sixth NRAO/NMIMT Synthesis Imaging Summer School. Edited by G. B. Taylor, C. L. Carilli, and R. A. Perley. ASP Conference

Series, Vol. 180, 1999, p. 171.
Bibliographic Code: 1999ASPC..180..171W

8. https://www.gb.nrao.edu/~rmaddale/Weather/.